5-1-1995

Spectral analysis of blood velocity in the human fetus

Francis J. Gallagher

Spectral Analysis of Blood Velocity in the Human Fetus

by

Francis J. Gallagher

A thesis Submitted
in
Partial Fulfillment
of the

MASTER OF SCIENCE

in

Mechanical Engineering

Approved by:

Mark H. Kempski, Ph.D. Department of Mechanical Engineering	_____ (Thesis Advisor)
Edward R. Salem, Ph.D. Department of Electrical Engineering	_____
Kevin B. Kochersberger, Ph.D. Department of Mechanical Engineering	_____
Charles W. Haines, Ph.D. Department of Mechanical Engineering	_____ (Department Head)

Department of Mechanical Engineering
College of Engineering
Rochester Institute of Technology
Rochester, NY 14623

May 1995

I, Francis J. Gallagher, hereby grant permission to the Wallace Memorial Library of the Rochester Institute of Technology to reproduce my thesis entitled 'Spectral Analysis of Blood Velocity in the Human Fetus' in whole or in part. Any reproduction will not be for commercial use or profit.

Francis J. Gallagher

5-12-95
Date

Acknowledgments

I would like to thank Dr. Mark Kempski for his support and encouragement.

I would also like to thank my parents Francis and Donna Gallagher, and my sister Laurie Gallagher, for their support and encouragement.

Contents

List of Figures

List of Tables

List of Charts

1 Introduction

Congenital cardiac malformations are a major health problem affecting the development of the fetal cardiovascular system. Currently there are no diagnostic tools that allow the assessment of fetal cardiovascular health early in pregnancy. We hypothesize that variances in heart rate and arterial and venous blood flow velocity correlate directly to fetal cardiovascular function[1]. Our goal is to develop a non-invasive measure of fetal cardiovascular health in the 10 to 18 week human embryo-fetus. This thesis focuses on the development of an automated computational algorithm to analyze arterial and venous Doppler velocity waveforms.

This section describes the long term and short term objectives of this project. Developmental aspects of the cardiovascular system in the human fetus will also be introduced. Finally, clinical problems which arise during cardiovascular development will be described briefly. The intent of this description is to provide the reader with some clinical perspectives.

1.1 Objectives

The long term objectives associated with this project are:

1) To develop a non-invasive measure of fetal cardiovascular well being.
2) To define operational norms for fetal cardiovascular function.

The short term objectives associated with this project are:

1) To develop an automated algorithm to analyze fetal blood velocity

waveforms.

2) To identify amplitude and frequency modulation characteristics associated with these waveforms.

Through the use of Doppler ultrasound, clinicians routinely monitor the fetal cardiovascular system non-invasively. Data gathered by Doppler ultrasound are analyzed to identify hemodynamic phenomena.

This thesis focuses on the development, testing, and documentation of computer algorithms vital to the digital acquisition, reconstruction, and primary analysis of Doppler velocity waveforms. Specific conclusions are deferred until a suitable data base is established.

A longitudinal and a cross-sectional study involving 200 and 300 patients, respectively is being conducted as part of a major inter-institutional study over the next 3-4 years. The longitudinal study will monitor individual patients during gestation and document post-partum outcome. The cross-sectional study monitors multiple patients at a specific gestational age. The results of this inter-institutional study will define the hemodynamic operational norms for the fetal cardiovascular system during primary cardiovascular development.

1.2 Cardiovascular Development

The fetal cardiovascular system is a biological system. This biological system has a unique performance envelope, just as a suspension bridge, a gasoline engine, and an F/A-18 aircraft possess unique performance envelopes.

A system operating outside its performance envelope usually indicates that there is a problem with the system. For example a suspension bridge may be subjected to violent oscillations of extraordinary magnitude. If the bridge was not designed to handle these oscillations it will succumb to a catastrophic failure. A gasoline engine may over-speed or stall when it is outside its performance envelope. This is an indication of a problem with the system itself, or with the system controller. In the case of the engine a simple tune-up may restore system performance.

The previous two examples illustrate what happens when a system operates outside its performance envelope. In one case the system was destroyed, in the other case a simple tune-up restored system performance. When a biological system operates outside its performance envelope this may indicate a departure from hemodynamic equilibrium. Sometimes something simple like aspirin will bring the system back within its performance envelope. At other times surgery may be necessary to restore system performance.

The computational algorithm described in this thesis provides data processing results that will be used in the cross-sectional, and longitudinal studies. These studies will establish the performance envelope of the fetal cardiovascular system during development. Eventually, these analysis techniques will be used to establish the bounds of normal cardiovascular function and fetal cardiovascular well being. Further diagnosis of abnormal cardiovascular function during fetal development may be possible with these

algorithms. Ultimately these algorithms may serve as both a diagnostic and treatment assessment tool for the clinician.

An algorithm has been developed for the analysis of hemodynamic waveforms, and is described later. The algorithm primarily identifies the amplitude and frequency modulation characteristics of blood velocity time series waveforms (see Results).

1.3 Clinical Perspective

The human heart begins development *in utero* as two simple tubes that fuse together to form a single heart tube. This heart tube forms and begins to pump blood by the 22nd day post-conception (Figure 1 adapted from Marieb)[2].

Figure 1

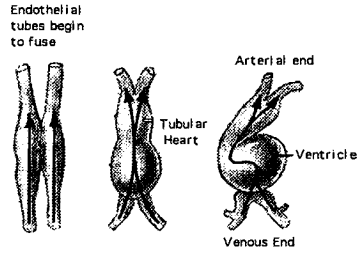

During the next three weeks, the embryonic heart is transformed from a muscle wrapped tube into a four chambered organ [2] (Figure 2 adapted from Marieb)[2].

Figure 2

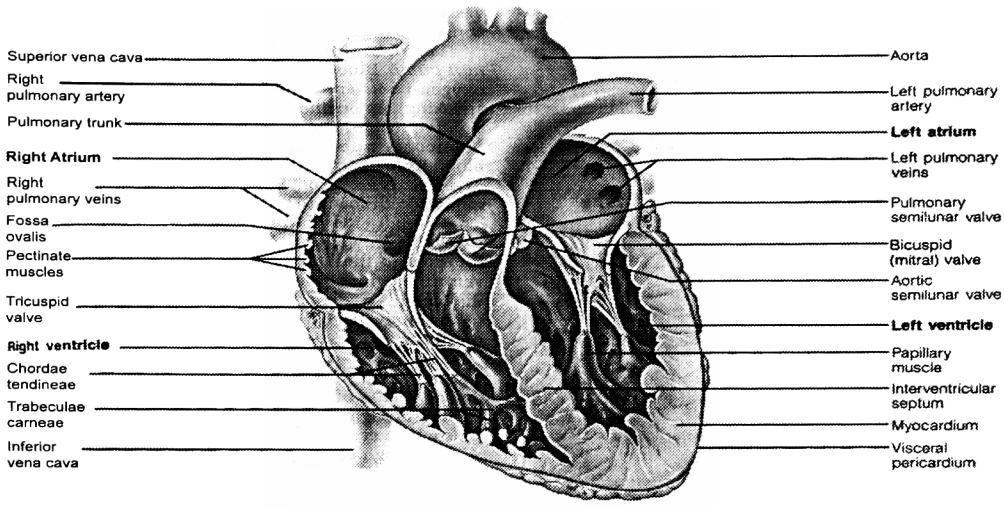

The heart is the first functioning organ in the fetus [3, 4]. The primary function of the heart is to deliver blood to the developing tissues and organs so that oxygen and nutrients necessary for growth and metabolism can be maintained. The pumping action of the heart also propels blood from peripheral tissues carrying metabolic waste products generated by the system (CO_2, etc.,) for removal.

Research into functional cardiovascular development is driven by several clinical imperatives:

1) Congenital cardiovascular defects are the single largest cause of infant mortality [5],
2) Congenital cardiovascular defects are diagnosed in 1% of all births affecting nearly 80,000 infants each year,
3) Before their first birthday 20% of the infants diagnosed with congenital

cardiovascular defects will be dead [5],

4) We need to define the causes and pathogenesis of congenital cardiovascular defects,

5) Pregnancy induced hypertension occurs in 10% of all pregnancies [1],

As pointed out earlier, we wish to establish a performance envelope for the fetal cardiovascular system, which allows the identification of clinical cases which fall outside the performance envelope. Evidence of congenital cardiovascular defects, or hypertension would be seen in the velocity profiles of an affected fetus. The intent of the computational algorithm developed in this thesis is to aid the identification of these cases through the development of signal processing tools which afford the clinician, greater diagnostic specificity and accuracy. Identified patients could be set aside for additional monitoring, and/or treatment.

For example, between 10 to 18 weeks gestation, the fetal vascular bed is transformed from a high flow resistance system to a low flow resistance system [1]. By establishing the operating norms (performance envelope) of the fetal cardiovascular system we can determine which fetuses are at risk. The at risk fetus could then be treated (in appropriate cases with low dosage aspirin therapy). In the case of congenital cardiovascular defects such as: ventricular-sepal defect, transposition of the great vessels, coarctation of the aorta, tetralogy of Fallot, or pulmonary stenosis [2], if functional malformations can be identified then explicit correction (surgery) can be prescribed, or implicit

correction coordinated via up-regulation of compensatory fetal hemodynamic mechanisms, where appropriate. Most congenital cardiovascular defects are traceable to environmental influences such as maternal infection, or drug use during the second month of pregnancy [2]. It is during this time that the human heart is transforming from a muscle wrapped tube into a four chambered organ.

Evidence of environmental and drug affects on the developing cardiovascular system can be found from studies done on chicken embryos. For example, when environmental temperature rises, a chick embryo's heart rate increases. When the environmental temperature is lowered, chick embryo heart rate decreases [6]. This phenomenon is observed in some of the data sets analyzed, during the course of this study. The velocity profile increases linearly over time indicating an increase in environmental temperature over time.

An example of adverse drug intervention on cardiovascular system development is seen in chicken embryos. Our colleagues in the Netherlands have treated some of there chick embryos with retinoic acid. This treatment is performed during the time when the embryonic heart is transforming from a muscle wrapped tube into a four chambered organ. Retinoic Acid treatment reliably produces embryos with double outlet right ventricles [7], and other anatomic and/or neurologic cardiovascular defects.

2 The Doppler Effect and Doppler Ultrasound

The fetal blood velocity data analyzed in our laboratory is gathered using a clinical Doppler ultrasound machine (Toshiba S-270). This section describes the fundamental physical and technical principles behind the Doppler effect, Doppler ultrasound, and the computational reconstruction of Doppler velocity waveforms.

2.1 The Doppler Effect:

The Doppler effect is a physical phenomena first explained by Christian Doppler in 1842[8]. The Doppler effect is caused by relative motion between a source and a receiver. Consider the classic case of a stationary receiver and a moving source. Assume that the source is the horn of an automobile. Assume that the receiver is a person standing on the side of a road. The car horn emits a sound at a particular frequency. As the car approaches the person, the apparent frequency (the frequency the receiver observes) is higher than the actual frequency of the horn. As the car moves away from the person, the apparent frequency of the horn is lower than the actual frequency.

The changes in apparent frequency described in the previous example can be quantified by the Doppler equation:

$$f_r = \frac{C}{C - V_s} \cdot f_s \qquad (2.1)$$

where f_r, is the frequency observed by the receiver, C, is the speed of sound in the transmission medium, V_s, is the velocity of the source, and f_s, is the

frequency transmitted by the source. When the source is moving toward the receiver, the ratio $C/(C - V_s)$ is greater than 1 (V_s is considered to be positive). Therefore the receiver observes a higher frequency. When the source is moving away from the receiver, the ratio $C/(C - V_s)$ is less than 1 (V_s is consider to be negative). Therefore the receiver observes a lower frequency.

Current technology makes use of the physical phenomena known as the Doppler effect in many instruments such as police radar, Doppler radar, and clinical Doppler ultrasound machines.

2.2 Doppler Ultrasound:

The ability to analyze blood flow using Doppler ultrasound has existed for over 30 years [9]. The use of Doppler ultrasound as a clinical diagnostic tool is popular because it is a non-invasive technique for analyzing blood flow in the cardiovascular system. The clinical Doppler ultrasound machine is a device used primarily to measure the Doppler effect. The Doppler ultrasound machine being used in this project is a pulsed wave Doppler system.

A pulsed wave Doppler system uses a sample volume. The flow that passes through the sample volume is analyzed to assess flow speed across the velocity profile. To analyze the flow velocity, the ultrasonic transducer emits a pulse which propagates through the biologic tissue of the patient being examined. Red blood cells reflect the pulses emitted by the ultrasonic transducer, which are received back at the same transducer working in 'receiver mode'. The distance from the transducer to the sample volume is determined

electronically, and the speed of sound through body tissue (C=1540 m/sec)[10] is known . The ultrasound machine determines the amount of time it will take for the pulse it transmitted to the sample volume to be reflected back. All of the echoes reflected by red blood cells not contained in the sample volume are filtered out. The remaining echoes represent pulses reflected back to the transducer by red blood cells contained in the sample volume. The velocity profile of the blood contained in the sample volume is determined electronically, and the Doppler equation is used to convert the frequency shift values into velocity values. The Doppler equation is given by the relation:

$$V = \frac{\Delta f \cdot C}{2 \cdot f_o \cdot \cos\theta} \qquad (2.2)$$

where V (m/sec), is the blood velocity, Δf (Hz), is the Doppler shift frequency, C, is the speed of sound in tissue (1540 m/sec), f_o (Hz), is the frequency transmitted by the ultrasonic probe, and θ (deg), is the inclusive angle between beam and blood flow directions, respectively. To get a true indication of the actual velocity, the angle between the probe and the flow should be as small as possible. As a rule the angle should be less than 20 degrees. The factor of 2 is introduced to take into account the fact that the transmitted pulse must make a round trip (from the probe, to the sample volume, and then back to the probe).

The echoes that are returned are converted to audio and video signals. The audio signal is a frequency modulated signal whose modulation frequency is proportional to blood velocity. In general, the audio signal can be written:

$$y(t) = \cos(\omega_o t + \beta \int x(t) \cdot dt) \qquad (2.3)$$

where ω_o, is the carrier frequency, x(t) is the modulating signal proportional to blood velocity, and β is a scale factor. Typically, the carrier signal is suppressed electronically within the clinical ultrasound machine prior to audio output. The audible signal is therefore the modulating signal, which is proportional to blood velocity through the Doppler shift equation (2.2). The audio signal allows the technician to hear the blood flow. The video signal allows the technician to view the blood flow.

If the direction of the blood flow is toward the probe, then the velocity profile will be displayed above the baseline, and the flow is considered positive flow (Figure 3).

Figure 3

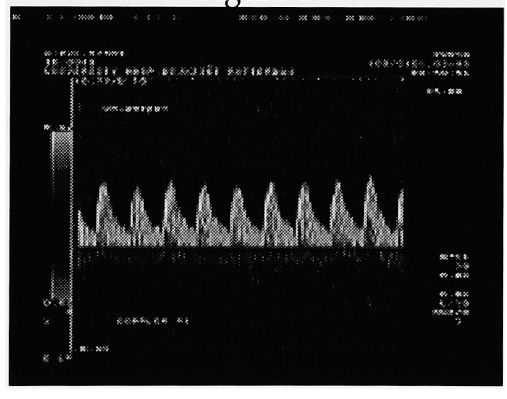

If the blood flow is going away from the probe, the velocity is considered to be negative, and the velocity profile is displayed below the baseline (Figure 4).

Figure 4

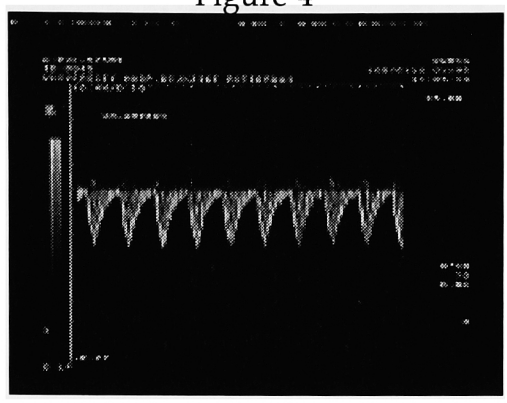

The video image of the velocity profile contains information pertaining to the characteristics of the flow. For example, a very intense (bright) image indicates that there is a lot of blood flowing through the sample volume. A dim image indicates the opposite. Also, an assessment of the flow, whether it is laminar or turbulent flow, can also be made. A smooth velocity profile indicates that the flow is laminar (red blood cells are speeding up, and slowing down together). A scratchy velocity profile is an indication of turbulent flow. In turbulent flow, blood does not flow in layers, rather it mixes, and the flow contains both low and high velocity components. Turbulent flow is usually caused by a narrowing of the vessel walls [8], and maybe an indication of disease as with atherosclerosis.

If blood vessel walls are present in the sample volume, echoes will be received. These echoes are very intense but are of low (Doppler shift) frequency, and represent the movement of the vessel walls. Since the blood velocity profile is of interest, a high pass filter, known as a 'wall filter' is employed to remove the low velocity wall movement.

A problem associated with pulsed wave Doppler systems is its inability to resolve blood velocities of large magnitude. This is due to the fact that the ultrasonic transducer sends out a pulse, and then must wait for the pulse to be reflected back from the sample before it can send out a new pulse. The rate at which the ultrasonic transducer can transmit a pulse, receive the reflected pulse and transmit a new pulse is the pulse repetition frequency [8]. The pulse repetition frequency is basically the sampling rate of the ultrasonic transducer. The Nyquist frequency is one half of the sampling rate (pulse repetition frequency)[11]. The largest resolvable velocity is equal to the Nyquist frequency scaled by the Doppler equation.

If the flow in the sample volume contains velocities that are above the Nyquist frequency, then aliasing will occur. When aliasing occurs in Doppler ultrasound measurement, a portion of the velocity profile gets clipped, and shows up as flow in the opposite direction. For example, if blood is flowing toward the probe (positive flow), with velocities that are above the Nyquist frequency, aliasing occurs, and the velocity components above the Nyquist frequency will show up as reverse flow. Figures 5 and 6 show the effects of aliasing on a Doppler video signal. The concept of aliasing is discussed in section 3.3.

Figure 5

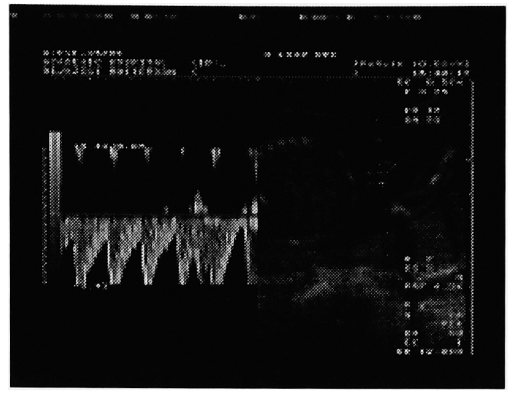

Figure 6

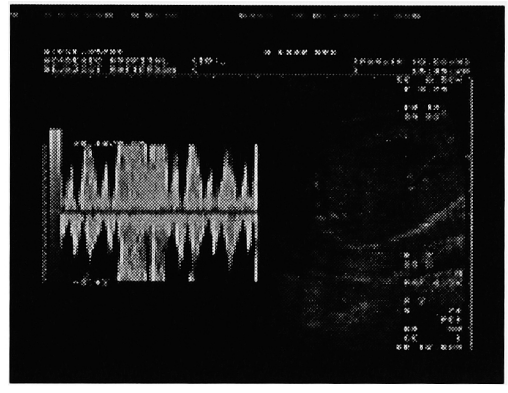

2.3 Doppler Velocity Reconstruction:

The Doppler blood velocity signals can be reconstructed from audio signals stored on video cassette tape. Recall from section 2.2 that the audio signal is the frequency modulating signal x(t) proportional to blood velocity. Spectral analysis of the raw audio signal has shown that there are no peaks of significant amplitude above 5 kHz. Peaks that occur above 5 kHz have amplitudes that are well below -40 dB. Figure 7 displays the instantaneous spectrum of the raw audio signal.

Figure 7

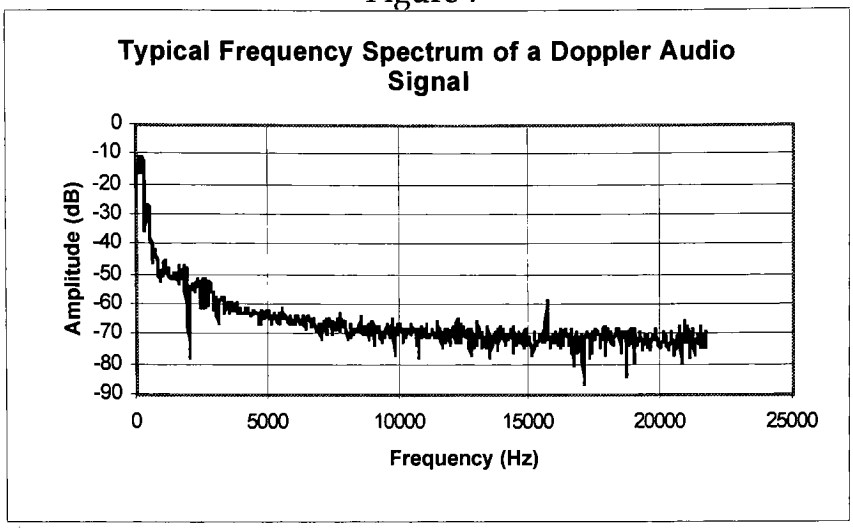

Here, the audio signal is sampled at 44 kHz, which results in a Nyquist frequency of 22 kHz. Note that the Nyquist frequency is well above the effective bandwidth of the signal.

The audio signal is digitally sampled, and these samples are stored in a data file. The original analog signal is now represented by a discrete sequence of sampled points. To reconstruct the blood velocity profile, the audio sequence needs to be demodulated. This is done by sequentially reading data 'packets' of sampled points from the file, and identifying the dominant frequency in the packet (see section 4.2, and Appendix D.2.2). The frequency at which the largest peak occurs is stored in a peak frequency array which is then scaled by the Doppler equation to digitally reconstruct the velocity profile.

2.4 Reconstructed Velocity Resolution:

The number of sampled points contained in a sampled data packet determines the data packet size. The algorithm used in this project requires that

the data packet size to be an integer power of 2 (for reasons discussed later). The data packets are read from a file, and are transformed from the discrete time domain into the discrete frequency domain. The size of the data packet that is transformed into the discrete frequency domain determines the frequency resolution assuming a fixed sampling rate. Each data packet read from the file contains N (N is a power of 2) sampled points. These points are equally spaced in time by the sampling period Δt (sec).

3 Digital Signal Processing

The ultimate goal of this project is to use non-invasive Doppler ultrasound techniques as a tool for diagnosing fetal cardiovascular well being. In order to define the characteristics associated with fetal cardiovascular homeostasis, a tremendous amount of data must be acquired, processed, and analyzed. This section addresses the digital signal processing (DSP) concerns associated with data acquisition, data processing, and data analysis. Several important topics involved in DSP are addressed:

- Sampling Theorem
- Nyquist Frequency
- Aliasing
- Frequency resolution and zero padding
- Leakage
- Windowing
- Amplitude Modulation (AM)
- Frequency Modulation (FM)
- Digital filtering (Butterworth low pass filters)
- Discrete Fourier Transform (DFT)
- Fast Fourier Transform (FFT)
- Spectral Representation of Data

It should be noted that the signals which are analyzed are assumed to be stationary. A signal whose statistical properties do not change over time is defined as a stationary signal [22].

3.1 Sampling Theorem:

The sampling theorem states that a band-limited analog signal can be uniquely determined by its sampled values. The sampled values are equally spaced in time, where the difference between two consecutive samples is the

sampling period Δt (sec). The sampling rate, f_s (Hz), is the inverse of the sampling period. The original analog signal can be reconstructed by the sampled values provided that the sampling rate, f_s, is greater than twice the highest frequency component in the band limited signal [23]. The largest resolvable frequency is known as the Nyquist frequency, f_n (Hz).

3.2 The Nyquist Frequency:

The Nyquist frequency is defined as that frequency which is half the sampling rate ($f_n=f_s/2$).

3.3 Aliasing:

If a sampled signal has frequency components above the Nyquist frequency, the original analog signal cannot be reconstructed from samples taken at $2 \cdot f_n$. The reason for this is that the Sampling Theorem was violated, and the signal has been aliased [23]. To understand aliasing, note that any signal can be represented as a summation of sinusoids. If we sample a sinusoid, and reconstruct it, we would need to acquire more than two points per cycle [24]. Inadequate sampling results in aliasing. The frequency components that lie above the Nyquist frequency will be folded over (about the Nyquist frequency). These high frequency components will appear to be low frequency components. That is, the aliased frequency components will appear to be low frequency components below the Nyquist frequency. Consider the following: a 4 kHz sinusoid is sampled at 6 kHz (the Nyquist frequency is 3 kHz). The

Sampling Theorem is not satisfied, therefore aliasing will occur. The 4 kHz sinusoid will appear to be a 2 kHz sinusoid.

3.4 Frequency Resolution and Zero Padding:

The frequency resolution one can expect to see in the frequency domain is determined by the value of Δf (Hz), $\Delta f = 1/(N \cdot \Delta t)$. The smaller the value of Δf, the better the frequency resolution and, hence, better velocity resolution. To increase resolution in the frequency domain, one can decrease the sampling period (Δt), or use more points in a data packet (N)[25]. Resolution in the frequency domain can also be improved by padding the data packets with trailing zeros (zero padding)[26]. Padding the data packet with trailing zeros increases the size of the data packet, and results in a smaller value of Δf.

3.5 Leakage:

A problem encountered in the frequency domain is spectral leakage. Leakage is caused by discontinuities in the data packet at packet leading edge and trailing edge boundaries, and the fact that there are only a finite number of frequencies in the discrete frequency domain [27]. The actual frequency content of the data contained in the packet is continuously distributed, but only quantifiable at discrete frequencies. The latter are constrained to be multiples of the lowest resolvable frequency, Δf. Therefore, some of the actual frequency content will be dispersed or "leaked" into neighboring frequency bins in an effort to best represent the frequency content of the data packet [28]. Also because

the signal is of finite duration, it will not be band-limited (it will be composed of sinusoids of all frequencies), this also contributes to leakage.

3.6 Windowing:

It was mentioned above that leakage is caused by boundary discontinuities in the data set. The effects of discontinuities can be lessened through the use of a smoothing window. The process of windowing involves point by point multiplication of the data packet by a window function. The window function contains the same number of points as the data packet. Multiplication in the time domain is equivalent to convolution in the frequency domain. Thus the frequency content of the data packet is convolved with the frequency domain representation of the window function. Proper choice of the window function can thus lead to a minimization of the 'leakage' effects caused by the finite window. The window used most often in this project is a Hanning window. The Hanning window is useful in resolving peaks in the frequency domain that are close together. A discrete time Hanning window can be generated using the relation[29]:

$$w[n] = \begin{cases} \frac{1}{2}[1 - \cos(\frac{2\pi n}{N})] & 0 \le n \le N \\ 0 & \text{elsewhere} \end{cases} \qquad (3.1)$$

Figure 8 shows the shapes of various windows in the time domain.

Figure 8

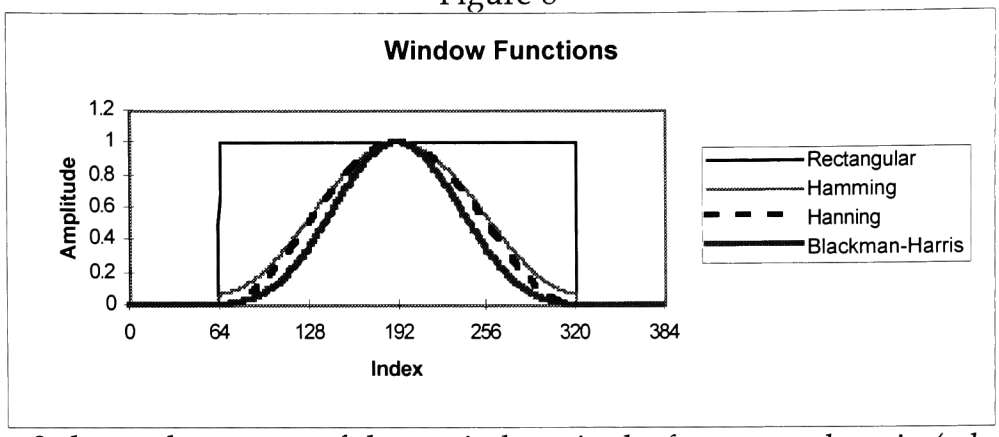

Figure 9 shows the spectra of these windows in the frequency domain (adapted from Textronix application note)[28].

Figure 9

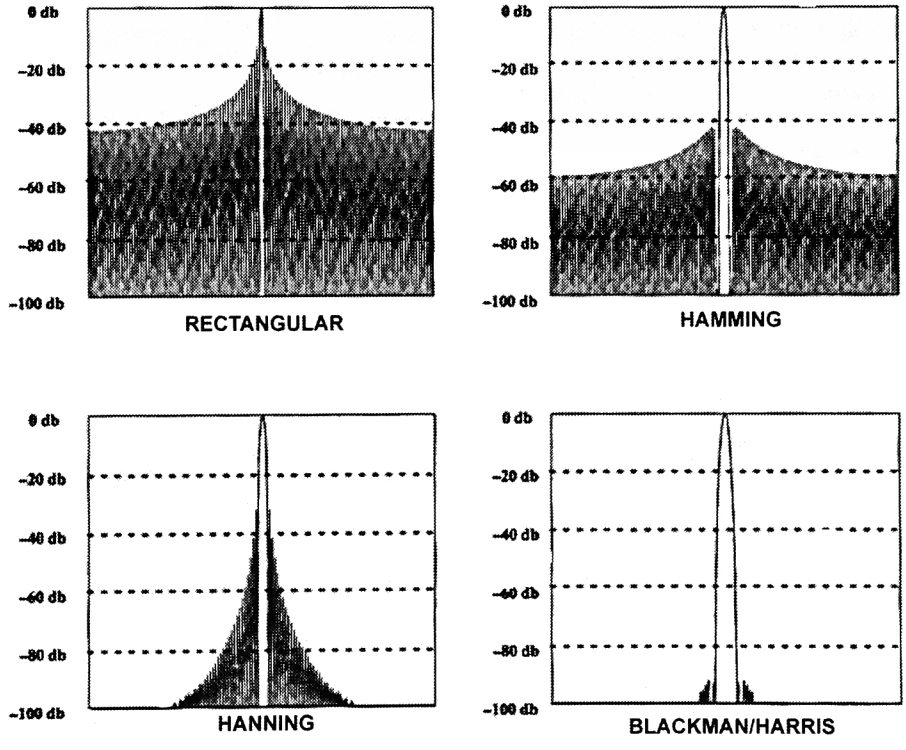

Note that the Hamming window has a broader main lobe than the rectangular window, but the side lobe structure has significantly lower magnitude.

3.7 Amplitude Modulation:

An amplitude modulation (AM) signal, is comprised of a carrier waveform, and a modulating waveform [30] in which the amplitude of the carrier waveform is modulated by the amplitude of the modulating waveform.

In section 5.3 we shall see that the blood velocity profile can be considered a carrier waveform. Velocity amplitude variability with time can therefore be considered modulating waveform.

3.8 Frequency Modulation:

A frequency modulated waveform consists of a carrier waveform, and a modulating waveform in which the instantaneous frequency of the carrier waveform is modulated by the amplitude of the modulating waveform [31].

In section 5.3 we shall see that variability in the cardiac cycle length (periodicity) or Heart Rate are frequency modulating waveforms.

3.9 Digital Filtering:

High frequency components present in the processed or analyzed waveforms are rejected by a 5th order low pass Butterworth filter. A low pass filter allows frequencies below the cutoff frequency to pass through, but it monotonically attenuates the frequencies above its cutoff frequency. An ideal filter has unity gain in the pass band and zero gain in the stop band. A

Butterworth filter is maximally flat, and approximates an ideal filter[32]. As the filter order increases, the approximation to an ideal filter becomes better and better. Butterworth filters of any order pass through -3 dB at the cutoff frequency. The last two properties of Butterworth filters are shown in Figure 10.

Figure 10

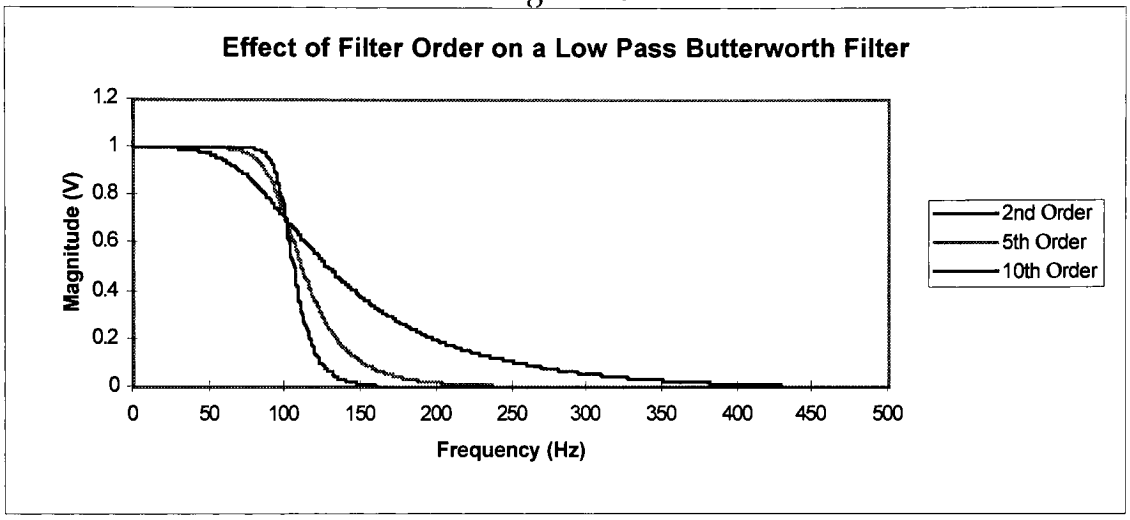

3.10 Discrete Fourier Transform:

The Discrete Fourier Transform (DFT) is a mathematical operation that transforms a sequence in the discrete time domain into a sequence in the discrete frequency domain. The DFT is given by the following relation:

$$X(k) = \sum_{n=0}^{N-1} x(n) \cdot e^{-j\frac{2\pi nk}{N}} \qquad k = 0,1,\ldots N-1 \qquad (3.2)$$

where x(n) is the discrete time sequence, X(k) is the discrete frequency sequence, and N is the number of points in the sequence. An important property of the DFT is that it is a linear operation.

3.11 Fast Fourier Transform:

The DFT is a very powerful tool however, it is a very computationally intensive algorithm. To evaluate an N point sequence using a DFT requires on the order of N^2 operations. For large values of N, calculation the DFT is very time consuming. An algorithm that produces the same result as the DFT, in a lot less time, is the Fast Fourier Transform (FFT). A common FFT algorithm requires that the discrete sequence be an integer power of 2. The FFT makes use of the fact that the DFT is a linear operation.

The FFT breaks the original sequence into two subsequences. The FFT algorithm continues to break down the subsequences until there are only two point DFTs to evaluate [29]. The results of the two point DFTs are used to compute the four point DFTs, and so on. This process continues until the entire DFT is calculated. The number of operations required to perform an FFT on a sequence of size N is on the order of $N \cdot \log_2(N)$ (compared to N^2 for the DFT)[29]. It is obvious that the FFT is a much more computationally efficient algorithm.

3.12 Spectral Representation of Data:

As indicated earlier, we are very interested in the spectral composition of the discrete hemodynamic variable time series. Aside from the processing of Doppler audio signals to construct blood velocity time series, the analysis of these velocity signals for intrinsic AM and FM characteristics, will ultimately allow for the establishment of criteria of normal fetal cardiovascular health.

The spectra of primary interest are the amplitude spectrum, the power spectrum, and the power spectral density (PSD). It should be noted that phase information is not contained in these spectra. When the FFT is calculated, both the magnitude and phase spectrum of the sequence are determined, and the reconstruction of the original discrete time series would require phase information.

The discrete power spectrum of each time series is computed using the following relation:

$$S_{xx} = \frac{FFT(x) \cdot FFT^{*}(x)}{N^2} \qquad (3.3)$$

where S_{xx} is the power spectrum, FFT(x) is the Fast Fourier Transform , $FFT^{*}(x)$ is the complex conjugate of the FFT, and N is the number of points in the sequence. If zero padding is performed on the sequence prior to calculation of the FFT, the power spectrum must be scaled by a factor of N^2/M^2, where N is the size of the zero padded sequence, and M is the size of the sequence prior to zero padding.

The amplitude spectrum of a sequence is simply the square root of the power spectrum. The only difference between the power spectrum and the PSD is that the PSD is divided by the quantity df (Hz). The units associated with the PSD are (magnitude)^2/(Hz). The PSD describes the amount of power contained in a sequence at a particular frequency.

The reason for using spectral analysis is simple, it allows one to identify the dominant frequency components contained in a signal. Figure 11 shows a series of sinusoids added together to form a complicated waveform. The equation of this waveform is:

$$x(t) = 10 \cdot \sin 2\pi(1)t + 5 \cdot \sin 2\pi(5)t + 3 \cdot \sin 2\pi(10)t + 5 \cdot \sin 2\pi(25)t \quad (3.4)$$

Figure 11

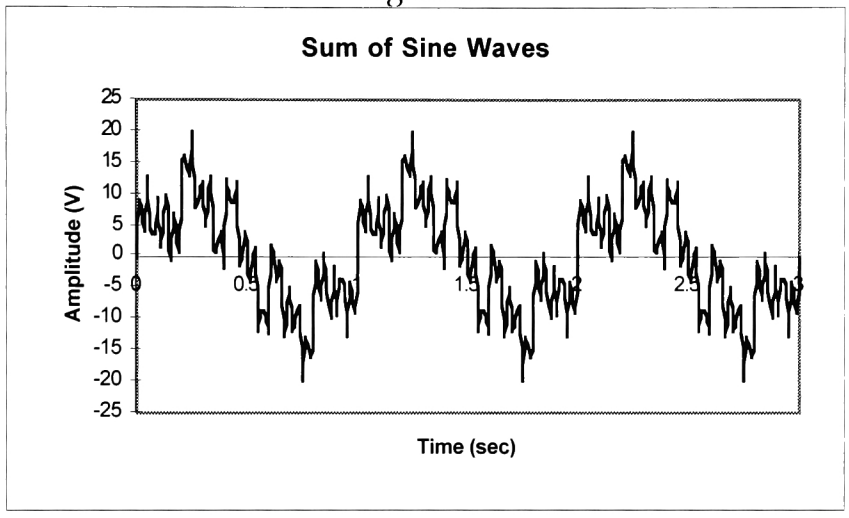

where the frequencies of the individual sinusoids in Hz are shown in parenthesis. As an analogy, consider Figure 12 where a group of coins is depicted in a pile.

Figure 12

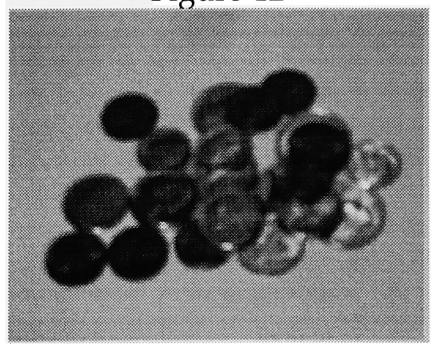

If we separate the coins into their various denominations, we find that there are 10 pennies, 5 nickels, 3 dimes, and 5 quarters. The coins sorted into their various denominations are show in Figure 13.

Figure 13

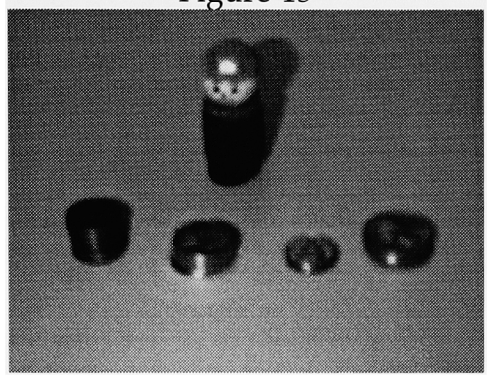

Similarly, if the complicated waveform of Figure 11 is sorted into the individual frequency components of which it is comprised, we find that there are peaks in the frequency spectrum at 1, 5, 10, and 25 Hz as shown in Figure 14. Note that the amplitude at respective frequencies matches that defined in equation 3.4.

Figure 14

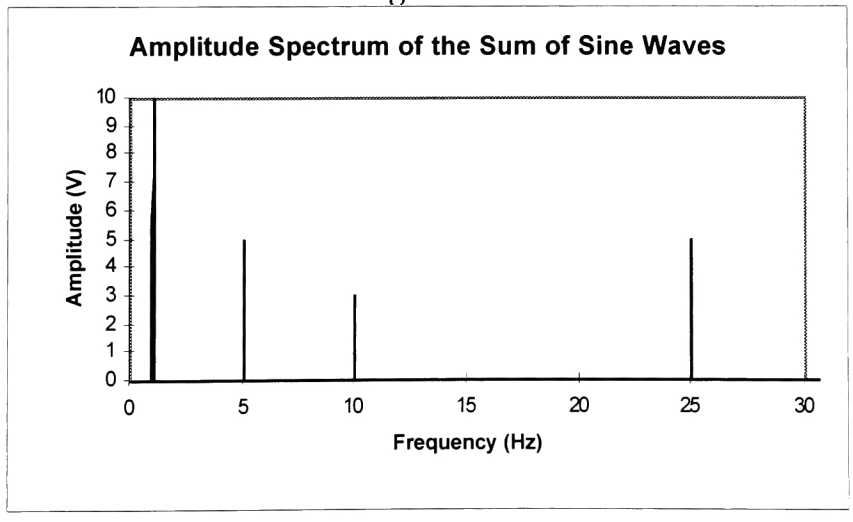

The point being made here is that although something may appear to be complicated, looking at it in a different way may provide some insight. This is why spectral analysis is useful.

4 Materials and Methods

4.1 Objective

The work associated with this project focuses on determining amplitude and frequency modulation characteristics of blood velocity waveforms in the human fetus, and chicken embryo. This section discusses the equipment and procedures used to acquire, process, and analyze blood velocity profiles. A description on how the human data is gathered will be given first. Next, the acquisition and processing procedures used to acquire and reconstruct the fetal velocity profiles is discussed followed by a similar discussion of the acquisition and processing procedures used on the chicken embryos. Finally, the AM/FM analysis performed on both the human and chicken data is described.

4.2 Human Fetal Data

The human fetal data is gathered using a Toshiba S270 clinical Doppler ultrasound machine by clinical colleagues at the Academic University Hospital-Rotterdam, in the Netherlands. To acquire the velocity data, the ultrasonic probe is focused on the vessel of interest (i.e., umbilical artery, uterine artery, descending aorta). The type of ultrasonic probe used depends on the age of the fetus. If the fetus is between the age of 10 - 14 weeks, a transvaginal probe (PVF 621 VT 6 MHz) will be used. If the fetus is older than 14 weeks a transabdominal probe (PVF 575 MT 5 MHz) will be used. In either case the measurements are non-invasive, and non-threatening to the maternal-fetal pair.

The Doppler image of the blood flow can be seen on a video monitor. The Doppler velocity profile is displayable as both a digital image (Figure 3) and an audio signal. The digital image and FM audio signal are recorded on a video tape. The audio signal is stored as a frequency modulated (FM) signal, where the modulating frequency is proportional to the blood velocity. Conventional VHS videotape is the recording medium for Doppler audio and video signals, which are subsequently sent to our laboratory for analysis.

When a tape is received, it is previewed and scrutinized for signals that are of appreciable duration (20 sec or longer) which have a high intensity velocity profile. Each recording on the tape is tagged with the following information: patient code, gestation, probe type, and blood vessel investigated. This information is used to categorize the processed data. We list the signals that have the characteristics noted above on a data sheet. The data sheet specifies the start time of the signal and its duration (in sec), the audio channel, the probe type, and the patient code, and the vessel. The patient code, and vessel information are used to specify file names. The signal duration and audio channel information is vital to the acquisition process.

To acquire the data from the video tape, the tape is played-back in a VCR (Panasonic AG-W1). The audio output from the VCR is routed to a connector block (National Instruments (NI) BNC 2081), and then to a data acquisition board (NI Lab PC+) inside a PC (Gateway P5-90). Using a custom data acquisition algorithm (NI LabVIEW 3.1 (see appendix for description)), the

frequency modulated audio signal is sampled at 44 kHz, and these samples are stored to a binary file.

The audio data we acquire is a frequency modulating signal whose frequency variation is proportional to blood velocity. To determine the frequency variation time series, the binary audio data is read sequentially from the file in 'packets'. A data packet consists of N (N is a power of 2) number of sampled points of the discretized audio signal by acquisition algorithm design. Using information contained in the file header, the binary data is then scaled to voltage data. Each packet is run through a Fast Fourier Transform (FFT) to determine its spectral content (this processing methodology is widely used)[12]. The frequency at which the largest peak amplitude occurs is retained, and represents the dominant frequency of that particular packet (see Chart 1). The magnitude of this peak is then compared to an intensity threshold (set by the user). If the peak magnitude exceeds the threshold, then the index at which the peak occurs is passed to the peak frequency array. If the peak magnitude is below the intensity threshold a value of zero is passed to the peak frequency array. Each of the data packets read from the file overlap the previous packet by at least 50 %. Overlapping is used to enhance data resolution [13]. The entire file is analyzed in this way, and the algorithm generates a 'peak frequency' array that is scaled by the Doppler equation to reconstruct the velocity time course. Figure 15 displays the demodulation and velocity profile reconstruction

process. A more detailed description of the demodulation process can be found in Appendix D.

Chart 1 - Velocity Reconstruction Flowchart

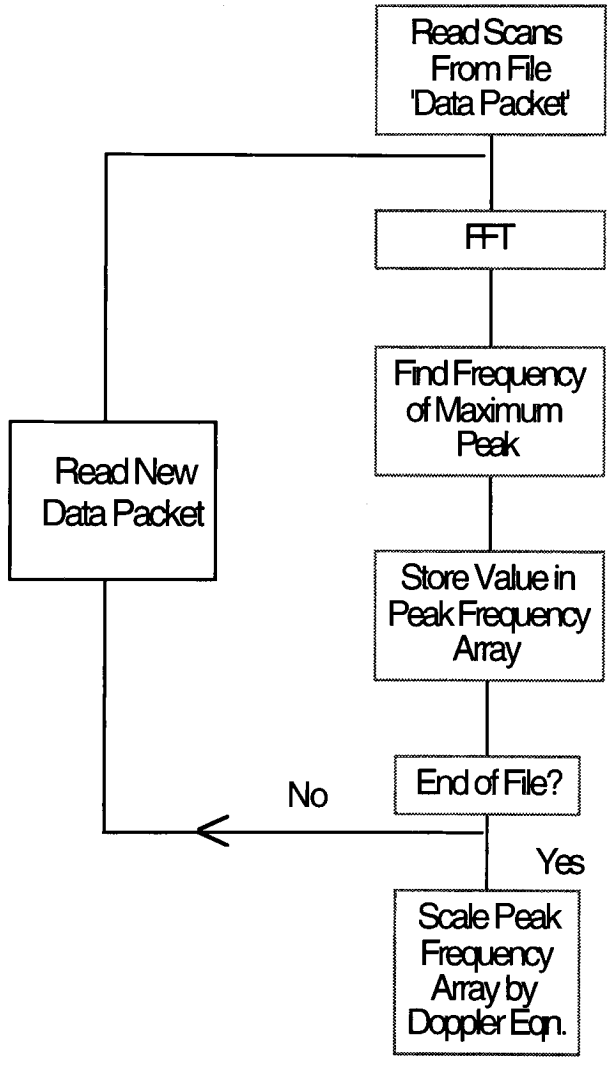

Figure 15

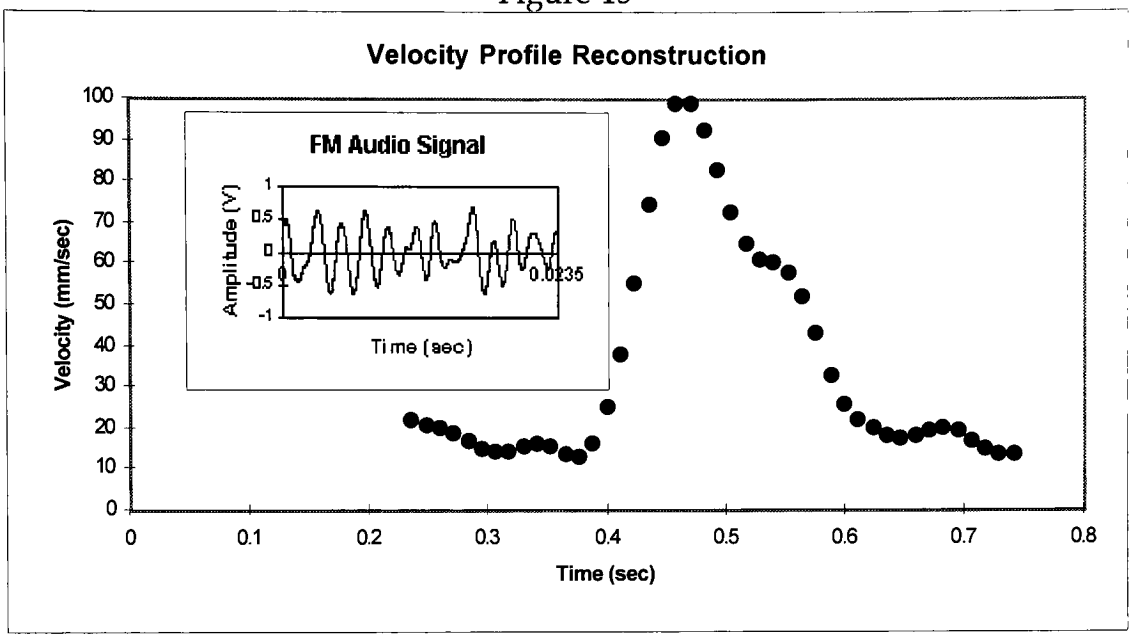

4.3 Chicken Embryo Data

The velocity profile of the blood flow in the dorsal aorta of chick embryos in various stages (stage 14, stage 16, stage 18, stage 21, stage 24, stage 27)[14] of development is also being studied, as a compliment/contrast to the human study. The velocity data is gathered using a 20 MHz directional pulsed Doppler velocity meter[15, 16]. To acquire the velocity data, the ultrasonic probe is focused on the dorsal aorta. The data was sampled at 5 msec intervals, for a duration of 100 sec. Here time and voltage proportional to the blood velocity is stored to an ASCII data file.

A custom LabVIEW Virtual Instrument (VI) maps the ASCII data to time and velocity data, and stores this information in a file format suitable for further analysis.

4.4 Generic Data Analysis

The reconstructed velocity profiles of the fetal or chicken blood flow velocity is analyzed in several ways, and the analysis procedure is the same for each. First, the mean value of the entire velocity waveform is computed. A threshold about the mean velocity value (set by the user) allows a custom LabVIEW VI to do peak detection and identify threshold crossings on the rising edge of the velocity waveform. Along with the reconstructed velocity profile, the algorithm generates arrays containing the peak velocity values and the times at which the peaks occur, the threshold crossings and the times at which they occur, and the mean velocity value per pulse.

The time between two consecutive peak velocity values and the time between two consecutive velocity threshold crossings are calculated. These values represent the peak time periodicity and the threshold crossing periodicity, respectively [17]. We construct two additional data sets from the peak time periodicity array, and the threshold crossing periodicity array. These data sets are the heart rate variability (HRV) time series based on peak timing, and threshold timing, respectively. Here, instantaneous heart rate is determined from the inverse period multiplied by 60 to yield beats-per-minute (BPM). The

periodicity and/or HRV data allow us to examine the frequency modulation characteristics of the blood velocity signal.

The peak velocity amplitude variance and the cardiac cycle mean velocity variance are defined by the difference in amplitude between two consecutive peak amplitudes, and two consecutive cardiac cycle mean velocities, respectively. Each of these data sets define different amplitude modulation characteristics associated with the velocity profile.

Each of the data sets described above undergo a uniform linear interpolation to yield new data sets that have N number of points (N is specified by the user), with uniform spacing with respect to time. The number of points to be interpolated is based on the duration of the original time series. This processing methodology has been used in previous studies [18, 19, 20, 21]. The ratio of the number of interpolation points to signal duration was between 25-50 (Hz).

The mean values of the interpolated data sets are then removed. If a trend exists in the data, it is removed through the use of a detrending routine (through the use of a linear, quadratic, or cubic polynomial). These detrended time series then undergo low pass filtering, zero padding, and windowing as required. The power spectra of the filtered (windowed, and padded) time series are calculated. The spectra are back corrected to remove any artifact encountered during the windowing.

The frequency and amplitude information for each spectrum is then passed to the sub VI *Normalized Spectra.VI*. The frequency axis of each spectra is normalized by multiplying the frequency array by the threshold crossing mean value. The periodicity spectra are normalized by dividing the periodicity by the threshold crossing mean value (sec). The heart rate spectra are normalized by dividing by the threshold crossing mean value (sec). The amplitude and mean cardiac cycle velocity are normalized by cardiac cycle mean value (mm/sec). To calculate normalized power spectral densities, the normalization factors for the amplitude values would be squared. The spectral information can be saved to file. These spectra allow us to identify the amplitude and frequency modulation characteristics of the velocity profile. All of the spectra can be saved to a file for further post processing.

5 Results

This section presents the results generated by the algorithm which was developed for this project. Identifying amplitude and frequency modulation characteristics associated with the Doppler velocity waveforms is a major focus of this project. Two test signals were crafted to verify that the program was working correctly.

5.1 AM Test Signal Analysis

The first test signal was an amplitude modulated signal. This AM signal was generated using an HP 33120A function generator. The carrier waveform was a sine wave having a sine amplitude of .5 V, and a frequency of 10 Hz. The modulating waveform was also a sine wave having a sine amplitude of .2 V and a frequency of 1 Hz (the depth of modulation was .4). The resulting AM signal was acquired and processed, using the algorithms developed for this thesis. Figure 16 displays the processed waveform.

Figure 16

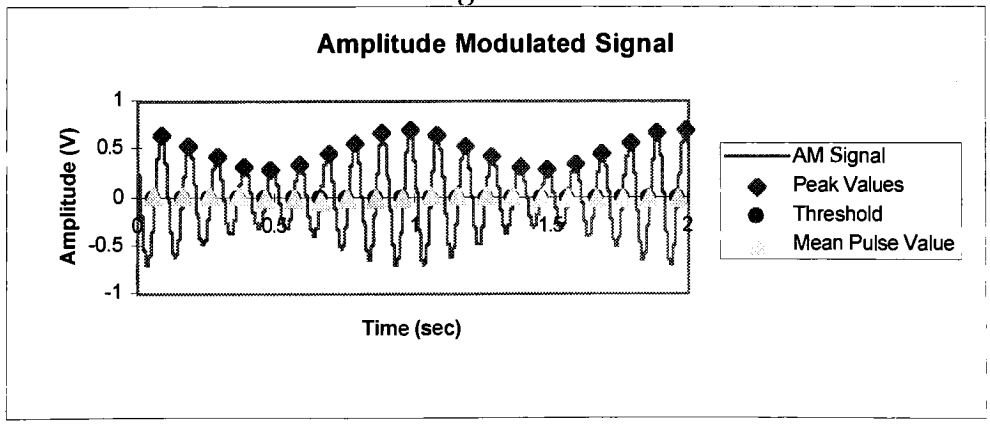

Of particular interest in this example are the diamond shapes which represent the peak amplitude values, and the triangles, which represent the mean pulse values. The two time series analyzed in this example are the peak voltage values diamonds '◆', and the mean pulse values triangles 'Δ'. Both time series were interpolated to 4096 points, detrended, and the resulting time series were filtered using a 5th order Butterworth low pass filter with a cut off frequency of 30 Hz.

Figures 17 and 18 display the AM Peak Voltage Variance, and AM Mean Pulse Value Variance time series, respectively. Note that the peak voltage and mean pulse value time series both have a frequency of 1 Hz, and sine amplitudes of .2 V, and .02 V, respectively. These amplitude values represent the variance* about the mean peak amplitude and mean pulse values, respectively.

Figure 17

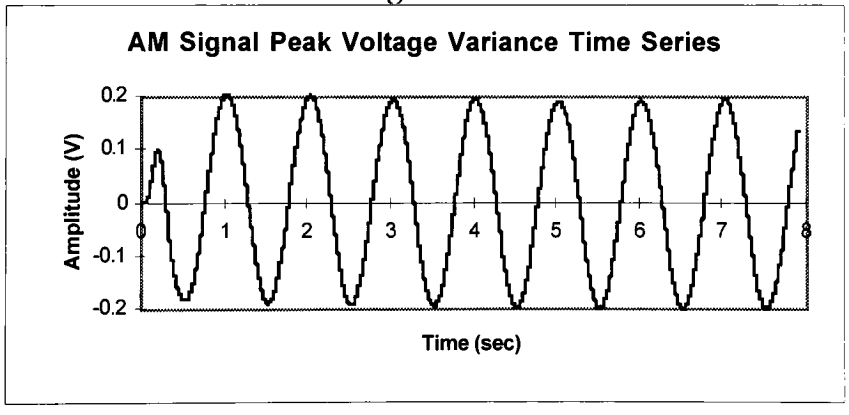

* In the current context the 'variance' describes the variability of the data series about its mean value. Variance in this context is not being used with statistical inference.

Figure 18

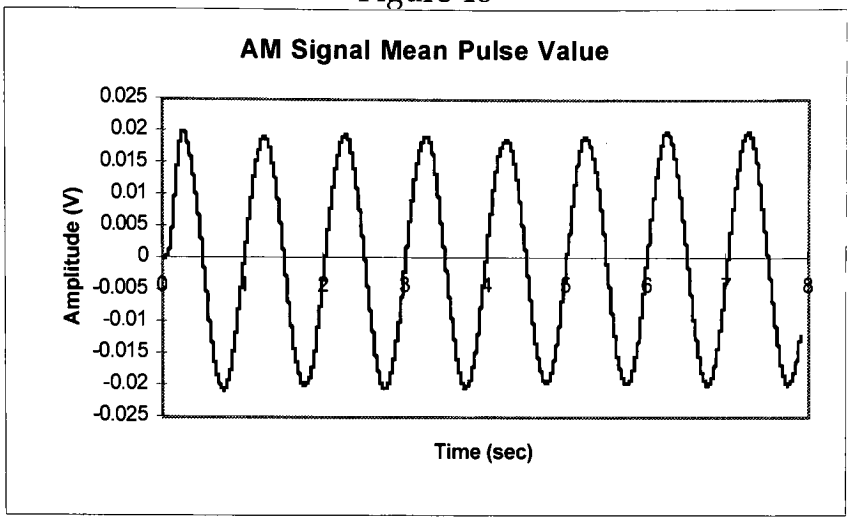

Figures 19 and 20 display the Amplitude Spectrum of the Peak Voltage and Mean Pulse Value time series, respectively. Note that the peaks in both spectra occur at 1 Hz. The peak amplitude in the Peak Voltage Variance spectrum (Figure 19) is approximately .18 V. The peak amplitude in the Mean Pulse Value Variance spectrum (Figure 20) is approximately .018 V. Leakage in the spectrum causes the peak amplitudes calculated in the spectrum to differ slightly compared to the actual amplitude values.

Figure 19

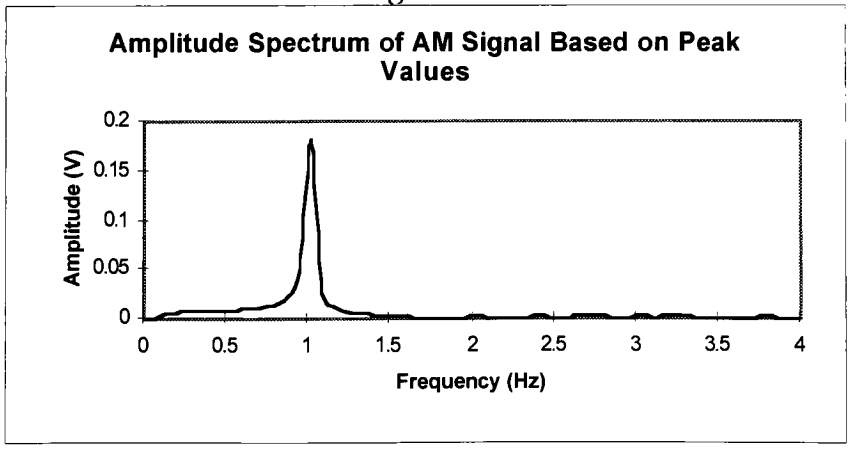

Figure 20

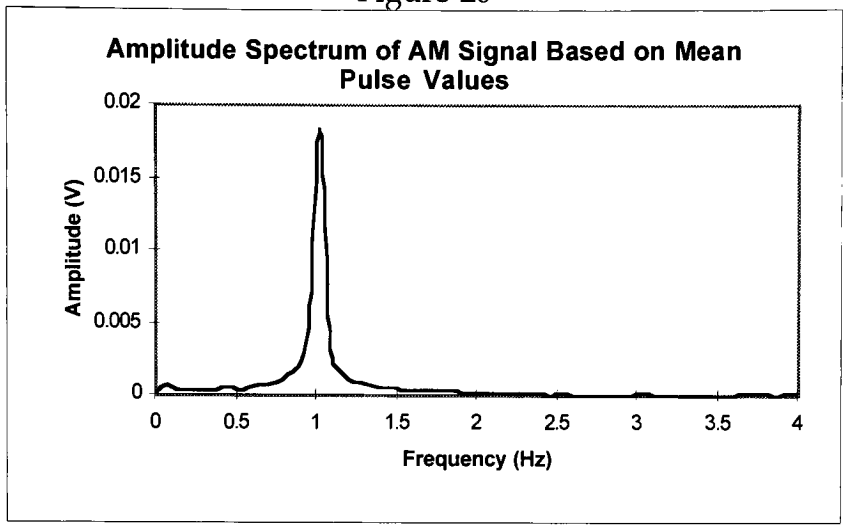

Figures 21 and 22 display the power spectral densities (PSDs) of Peak Voltage Variance, and Mean Pulse Value Variance time series, respectively. Note that the peak frequency occurs at 1 Hz in both spectra. The amplitudes of the peaks in the Peak Voltage Variance spectrum and Mean Pulse Value Variance spectrum are .52 V^2/Hz, and .052 V^2/Hz, respectively. The value of df in both spectra was 0.063 Hz. To determine the sine amplitudes, the peak magnitude is multiplied by df, then taking the square root of the resulting product yields the sine amplitude. These calculations were made, and yielded sine amplitudes of .18V, and .018 V for the Peak Voltage Variance, and Mean Pulse Value Variance time series, respectively. Again leakage in the spectrum accounts for the difference in amplitude.

Figure 21

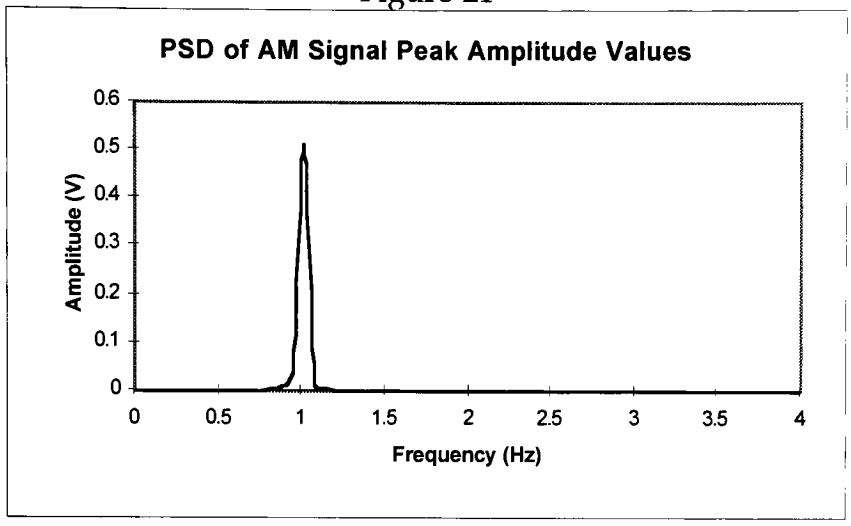

Figure 22

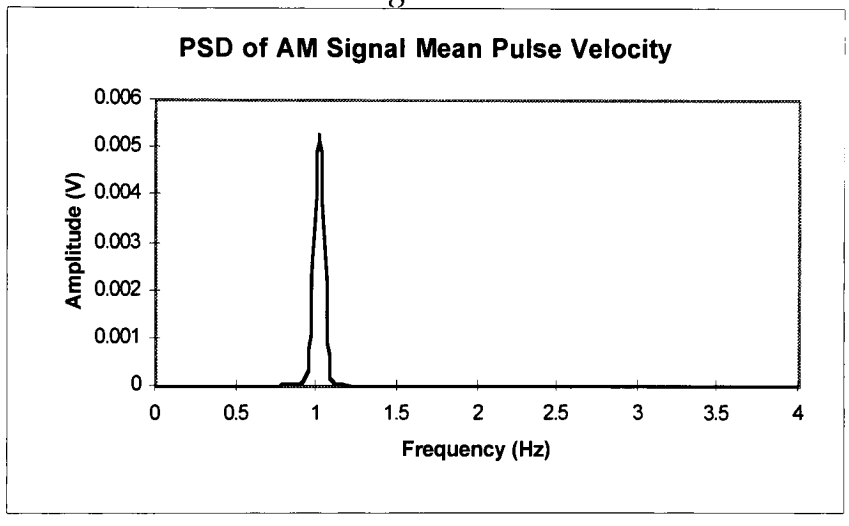

5.2 FM Test Signal Analysis

The second test signal generated was a frequency modulated (FM) signal. The carrier waveform was a sine wave with a sine amplitude of 1 V, and a frequency of 20 Hz. The modulating waveform was a sine wave with a sine amplitude of 1 V, and a frequency of 5 Hz. The maximum frequency deviation from the carrier frequency was 5 Hz. The FM signal was acquired and

processed. The processed waveform is displayed in Figure 23. The points of interest are represented diamonds '◆', and the circles '●' as displayed in Figure 23. The diamonds represent the times at which the peak amplitude occur, and the circles represent the times at which the user defined threshold is crossed.

Figure 23

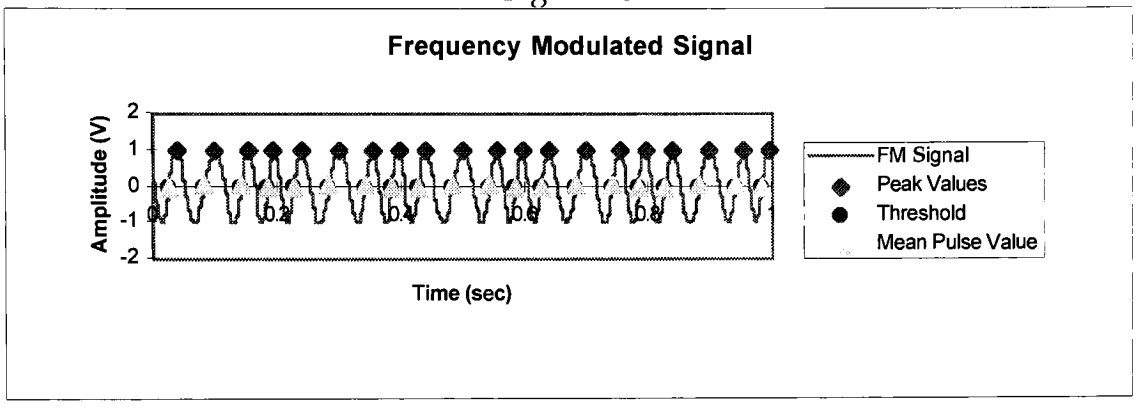

The Peak Periodicity time series is defined by determining the difference in time between two consecutive peak times. The Threshold Crossing Periodicity time series is defined by determining the difference in time between two consecutive threshold crossing times. These time series were interpolated to 4096 points, detrended, and filtered using a fifth order Butterworth low pass filter with a cut off frequency of 10 Hz.

Figures 24 and 25 display the Peak Periodicity Variance, and Threshold Crossing Periodicity Variance time series, respectively. The Peak Periodicity Variance time series has a frequency of 5 Hz, and a sine amplitude of approximately .0094 sec. The Threshold Crossing Periodicity Variance time series has a frequency of 5 Hz, and a sine amplitude of .0082 sec. These

amplitudes represent the variance about the mean peak periodicity, and threshold crossing periodicity values, respectively.

Figure 24

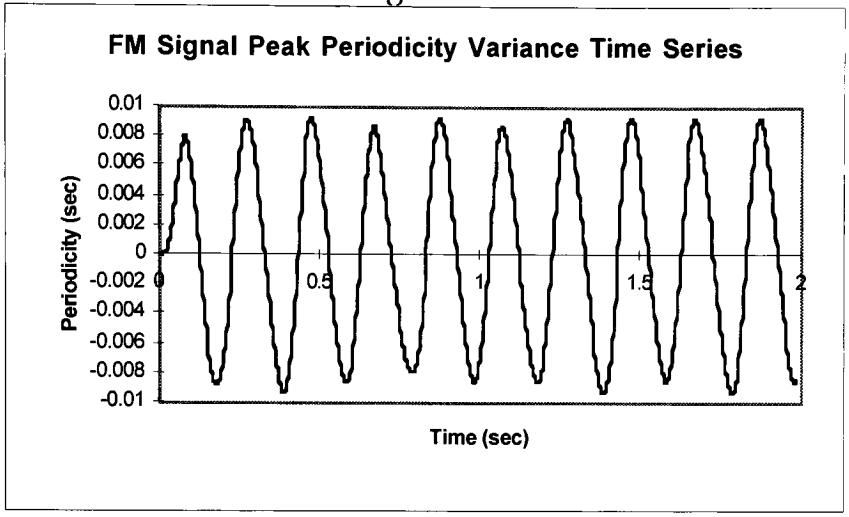

Figure 25

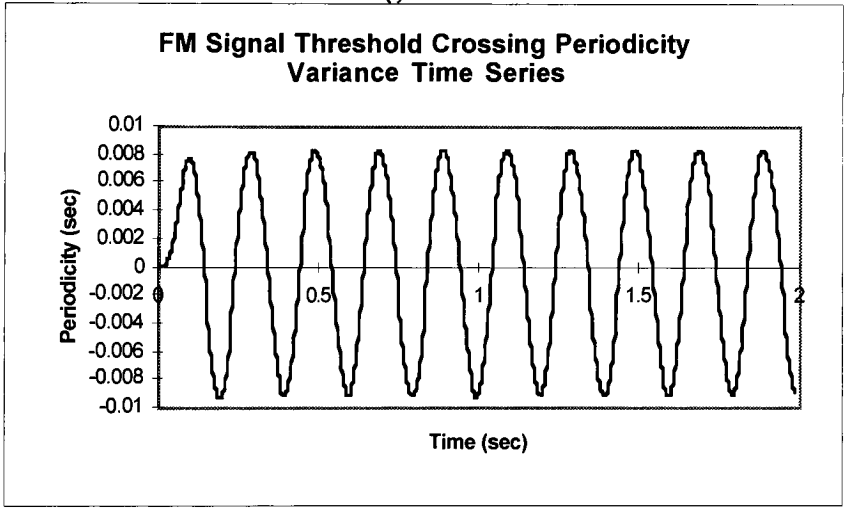

Figures 26 and 27 show the PSDs of the Peak Periodicity Variance, and Threshold Crossing Periodicity Variance, respectively. The peak in the Peak Periodicity Variance spectrum occurs at 5 Hz, and has an amplitude of .00065 sec^2/Hz. This corresponds to a sine amplitude of .0064 sec. The peak in the

Threshold Crossing Periodicity spectrum occurs at 5 Hz, and has an amplitude of .00063 sec^2/Hz. This corresponds to a sine amplitude of .0063 sec. The sine amplitudes are somewhat off due to the leakage in the spectrum, and the variation in the amplitude of the Peak Periodicity time series (see Figure 24).

Figure 26

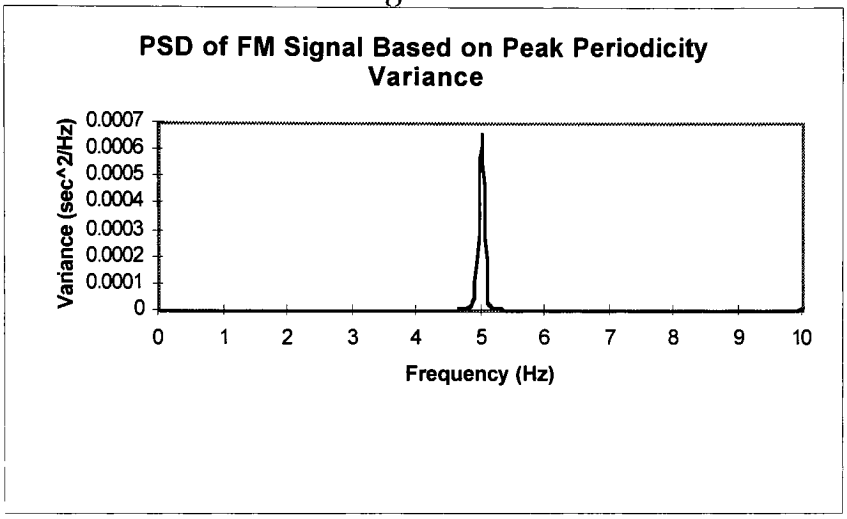

Figure 27

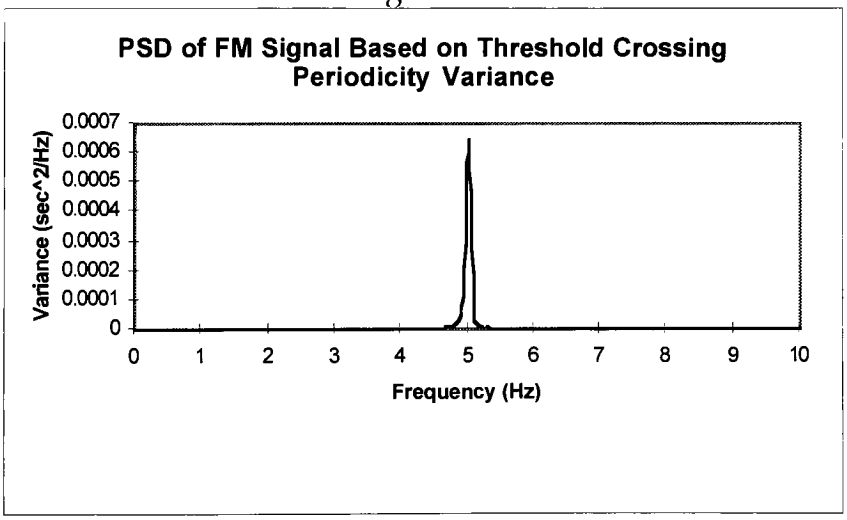

Figures 28 and 29 display the amplitude spectrum of the Peak Periodicity Variance, and the Threshold Crossing Periodicity Variance time series,

respectively. The peak in Figure 28 occurs at 5 Hz, and has a magnitude of .0064 sec. The peak in Figure 29 occurs at 5 Hz, and has a magnitude of .0063 sec. Again the magnitudes are off due to leakage in the spectra, and fluctuations in the amplitude of the defined time series (Figure 24).

Figure 28

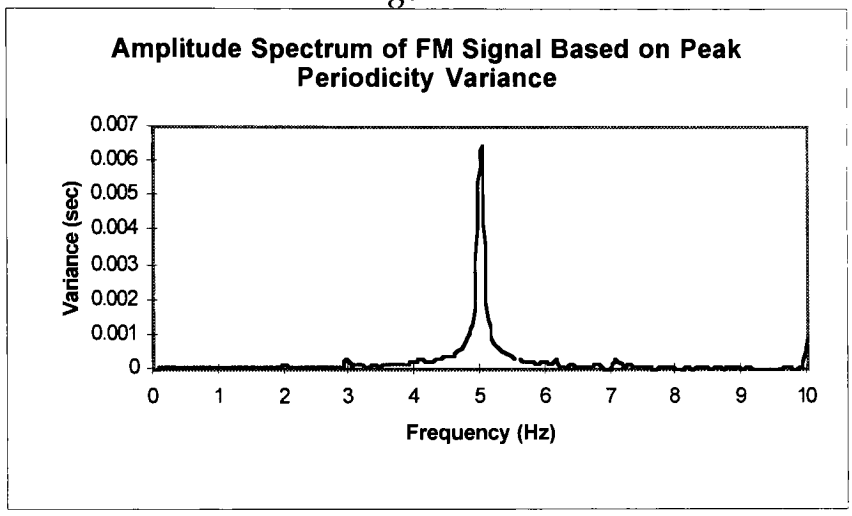

Figure 29

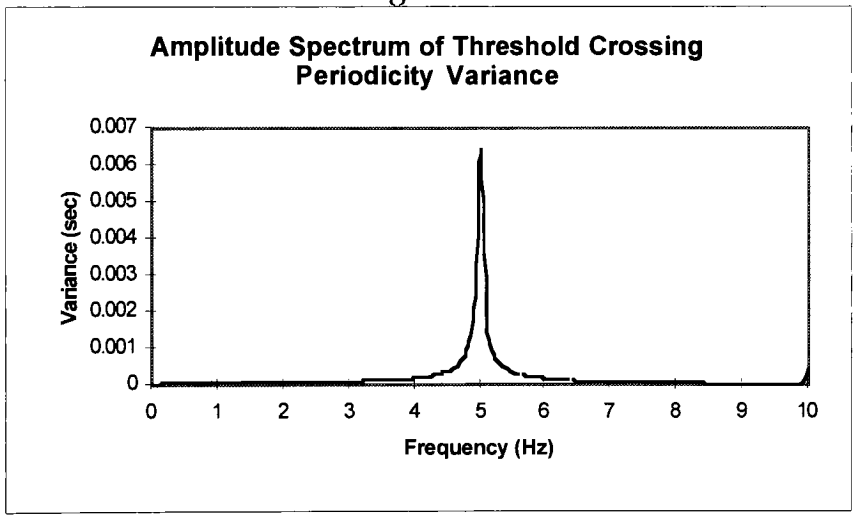

Figures 30 and 31 display the amplitude spectra of both the Peak Periodicity Variance, and the Threshold Crossing Periodicity Variance time

series subjected to a Hanning window, respectively. The peak in Figure 30 occurs at 5 Hz, and has a magnitude of .0079 sec.

Figure 30

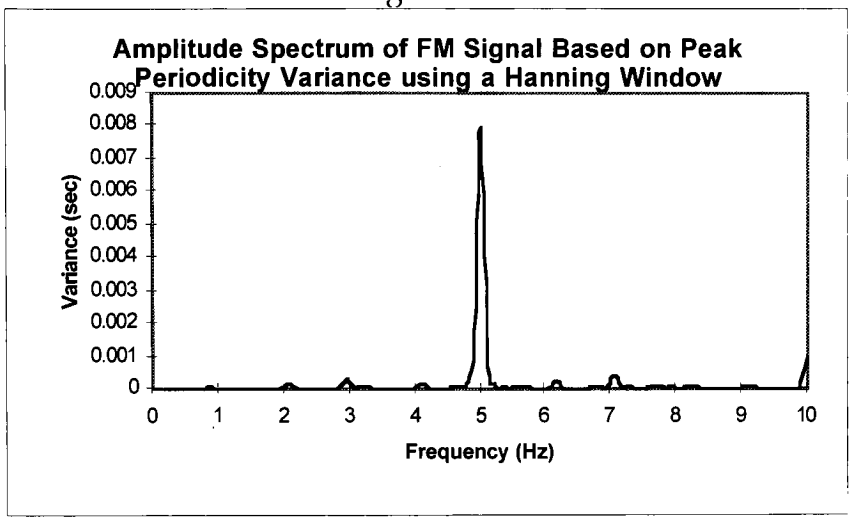

Figure 31

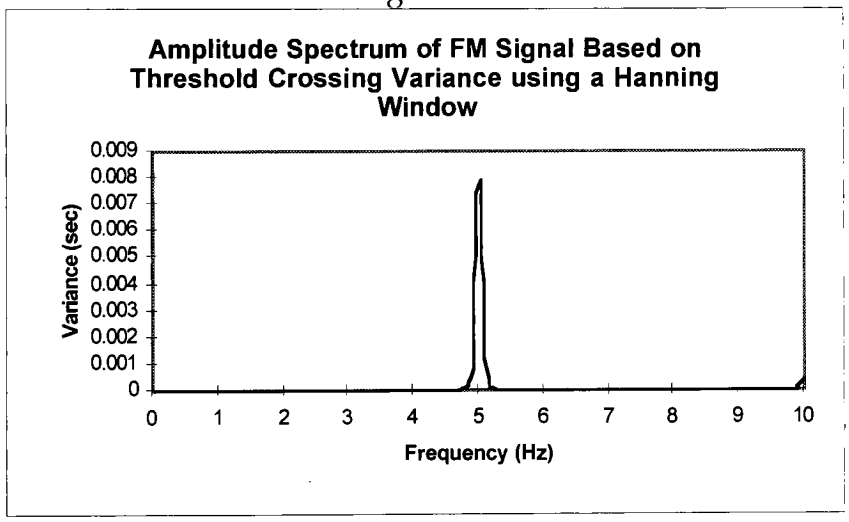

The peak in Figure 31 occurs at 5 Hz and has a magnitude of .0078 sec. Note that the amplitude and frequency values obtained from Figure 31 correspond very well with the Threshold Crossing Periodicity Variance time series. Again the magnitude of the peak corresponding to the Peak Periodicity Variance is

somewhat off. Since leakage is minimized through the use of the window, we can conclude that the amplitude fluctuation of the Peak Periodicity Variance plays a significant role in the actual amplitude, and measuring the amplitude over one cycle is not an accurate measurement. Note also that the Threshold Crossing Periodicity Variance Values are not affected by the magnitude fluctuations.

5.3 Physiologic Waveform Analysis

One of the main objectives of this project is to identify amplitude and frequency modulation characteristics of Doppler velocity waveforms. Figure 32 displays 6 sec of 30 sec duration blood velocity profile in the umbilical artery of a 10 week old human fetus.

Figure 32

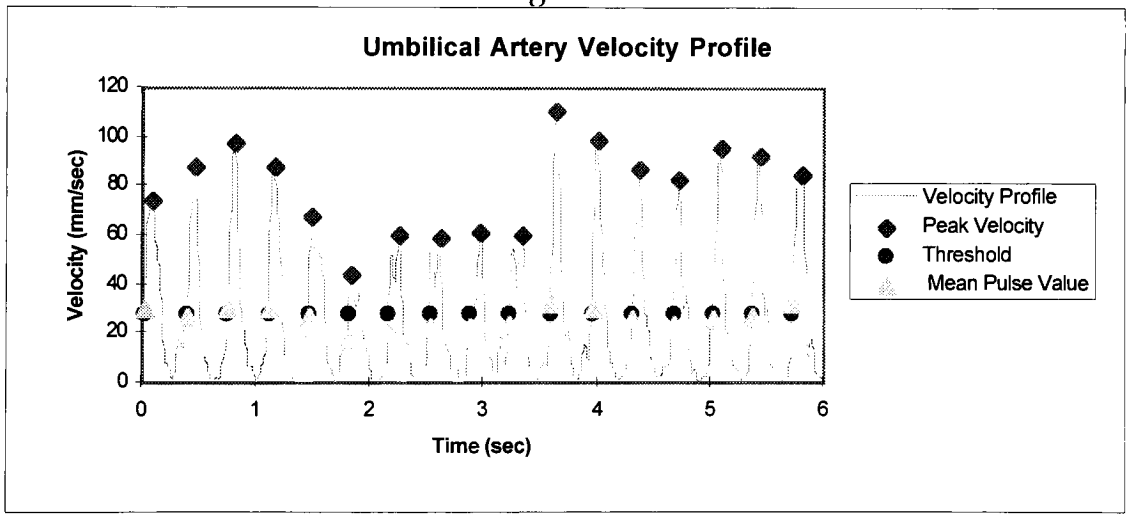

The diamonds '◆' indicate the peak blood velocity (mm/sec) amplitude values of each pulse. The triangles 'Δ' indicate the cardiac cycle mean velocity value (mm/sec). These markers define the Peak Velocity Amplitude Variance, and the

Cardiac Cycle Mean Velocity Variance time series, respectively. Figure 33 displays the entire Peak Velocity Amplitude Variance time series. Figure 34 displays the entire Cardiac Cycle Mean Velocity Variance time series.

Figure 33

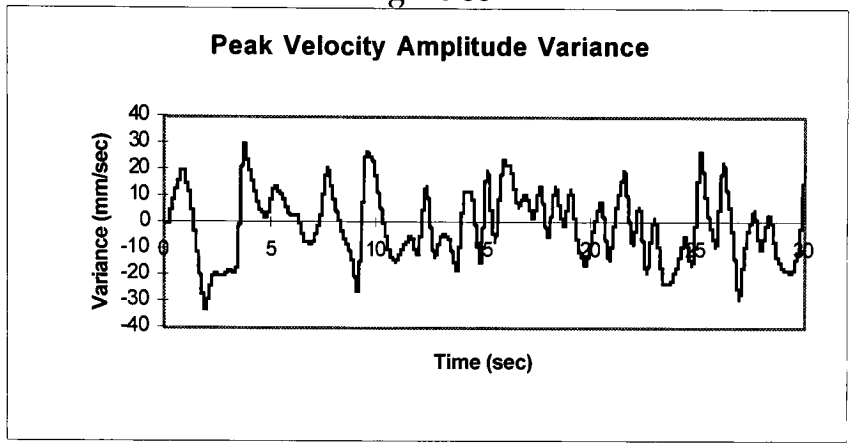

Figure 34

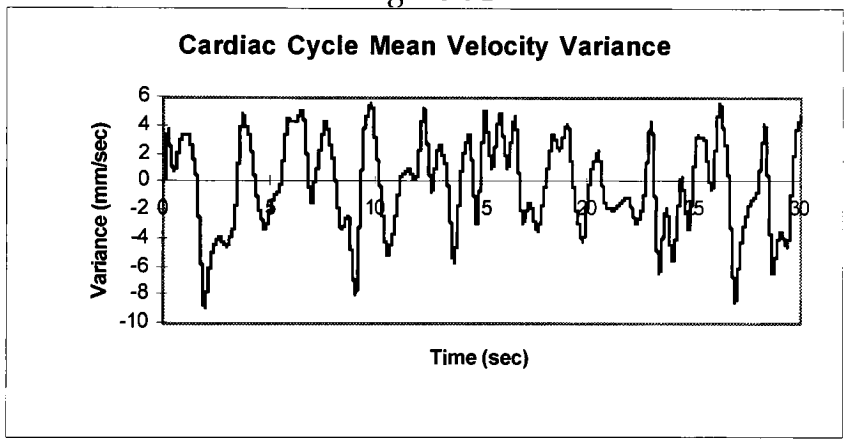

These two time series define the amplitude modulation characteristics of the velocity profile. The diamonds of Figure 32 also indicate the times at which the peak velocities occur, and the corresponding circles '●' identify the times at which the user specified threshold is crossed. These markers are used to define

the Peak Periodicity Variance, and Threshold Crossing Periodicity Variance time series, respectively.

Figures 35 and 36 show the Peak Periodicity Variance and Threshold Crossing Periodicity Variance time series, respectively. The peak periodicity is defined as the difference in time between two consecutive peak values. The threshold crossing periodicity is defined as the difference in time between two consecutive threshold crossings.

Figure 35

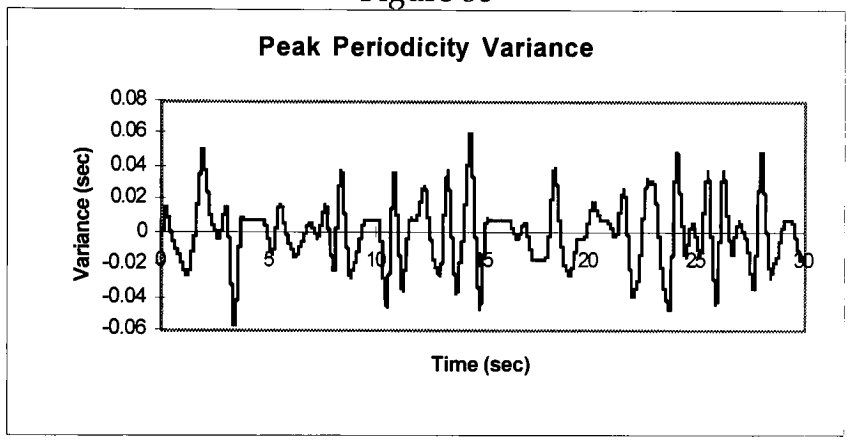

Figure 36

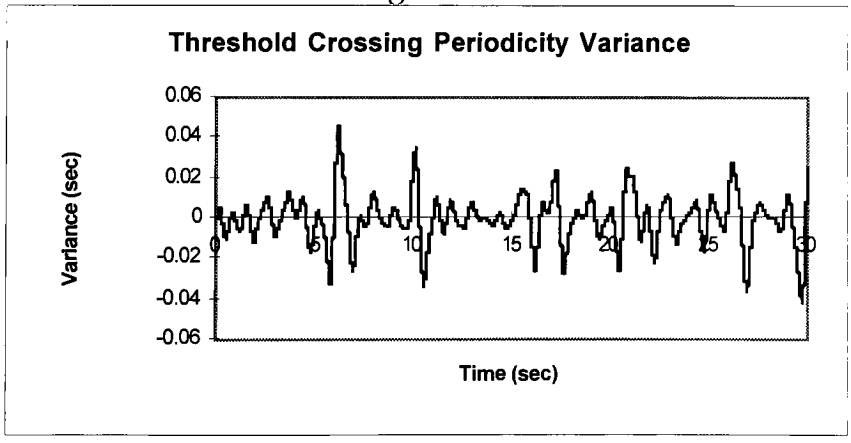

Figures 37 and 38 display the Heart Rate Variance based on Peak Periodicity values, and Heart Rate Variance (in beats-per-minute, BPM) based on Threshold Crossing Periodicity, respectively. These time series are generated using the peak periodicity time series, and threshold crossing periodicity time series, respectively.

Figure 37

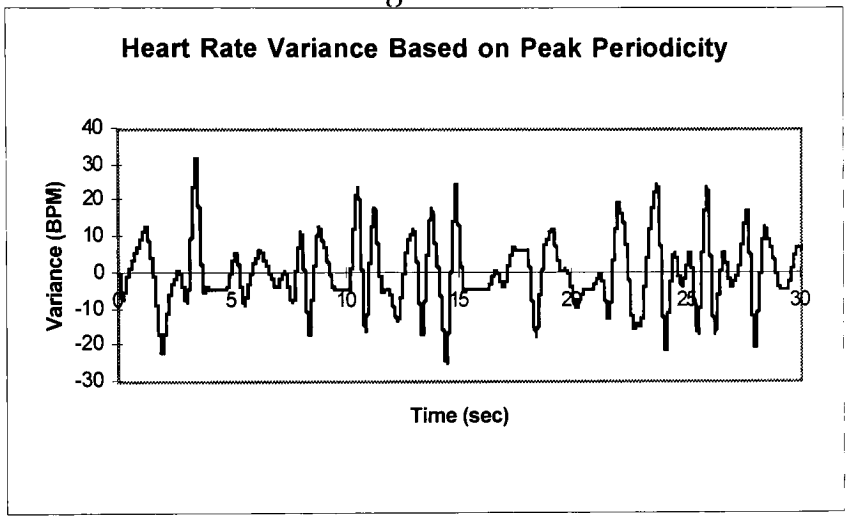

Figure 38

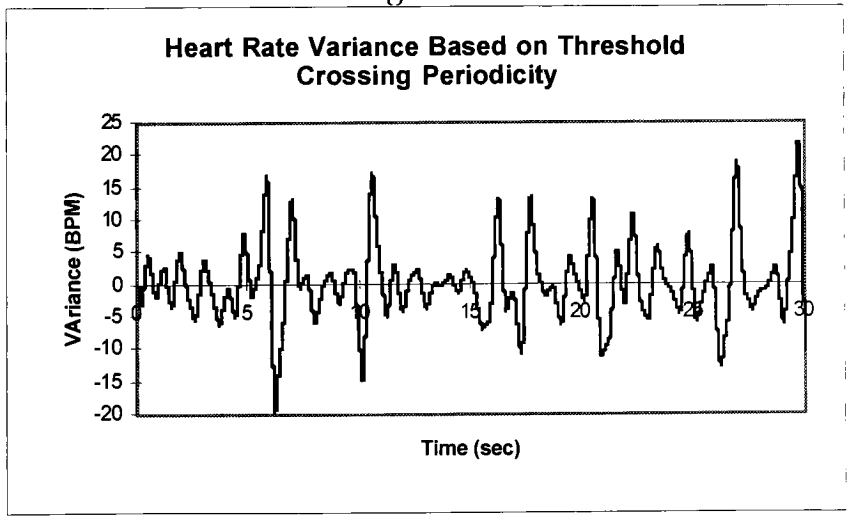

The reciprocal of the periodicity values are determined, and then are multiplied by 60 to obtain instantaneous heart rate in beats per minute (BPM). The Peak Periodicity Variance, Threshold Crossing Periodicity Variance, and the Heart Rate time series identify the frequency modulation characteristics of the blood velocity profile. All of the time series represent the variance about the their respective mean values.

Figure 39 displays the PSD of the Peak Velocity Amplitude Variance time series. Note that the dominant peaks in the spectrum occur at .189 Hz, and .48 Hz. This means that the two dominant sinusoids in the Peak Velocity Amplitude Variance time series have frequencies of .189 Hz, and .48 Hz, respectively. Figure 40 displays the PSD of the Cardiac Cycle Mean Velocity Variance time series. There are four dominant peaks in this spectrum occurring at .157 Hz, .314 Hz, .44 Hz, and .53 Hz respectively. Note that these spectra are approximately band limited to 1 Hz. The PSDs in Figures 39 and 40 represent the AM characteristics of the blood velocity profile.

Figure 39

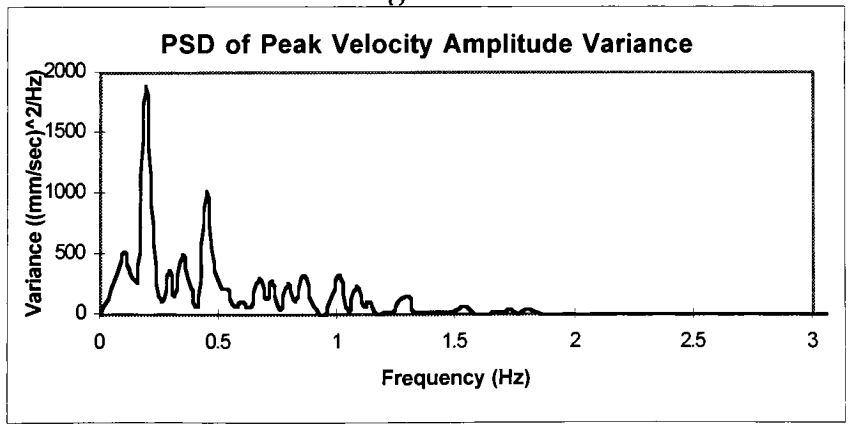

Figure 40

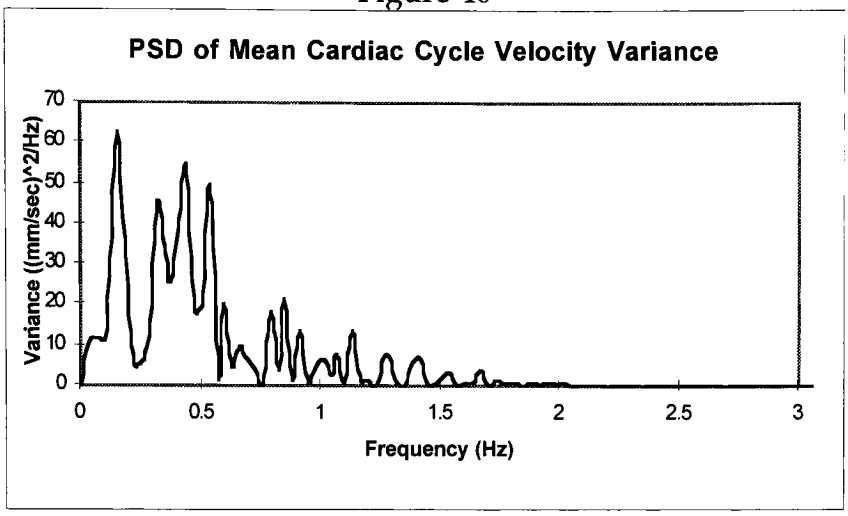

Figure 41 displays the PSD of the Peak Periodicity Variance time series. The dominant peaks occur at frequencies of .76 Hz and .819 Hz, respectively. Figure 42 shows the PSD of the Threshold Crossing Periodicity Variance time series.

Figure 41

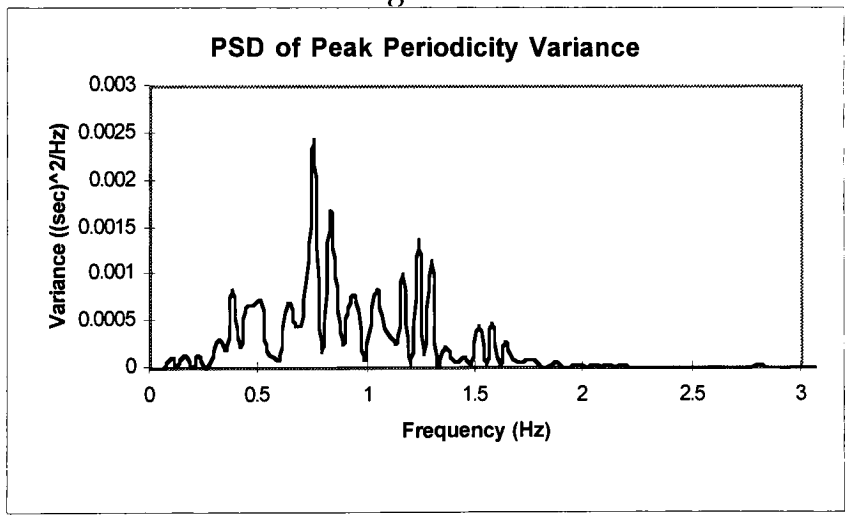

Figure 42

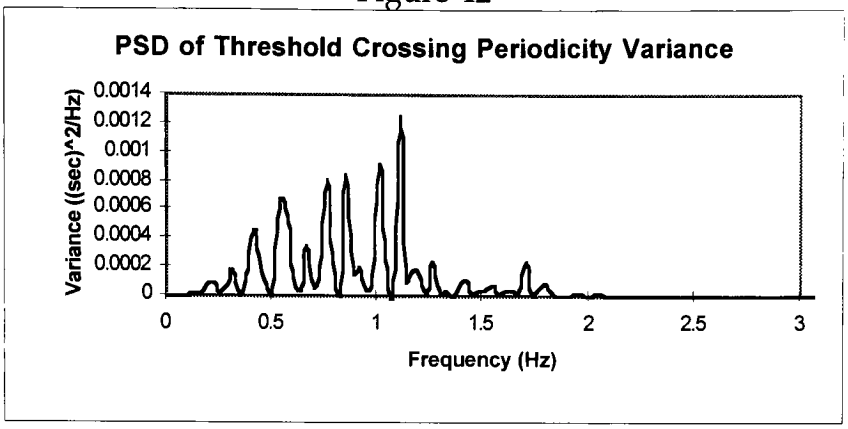

Figures 43 and 44 display the PSDs of the Heart Rate Variance based on Peak Periodicity Variance, and Threshold Crossing Periodicity, respectively. Because these time series are generated from the periodicity time series the dominant peaks will occur at the same frequencies as the periodicity spectra. The only difference between the spectra will be in the amplitude values. Figures 41, 42, 43, and 44 represent the FM characteristics associated with the velocity profile. Note that the FM spectra are band limited to approximately 1.5 Hz.

Figure 43

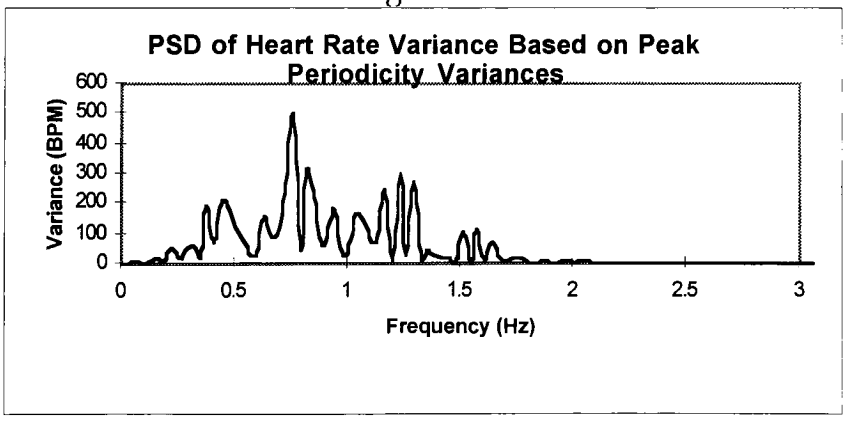

Figure 44

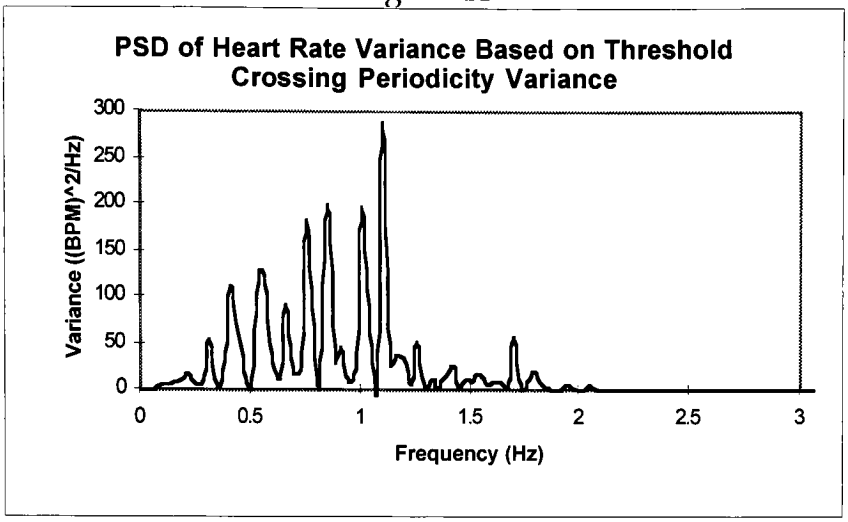

Note that physiologic interpretation of the aforementioned spectra is to be established from norms based on data amassed from several hundred patients over the next 3 years as part of the on-going Specialized Center of Research (SCOR)[1]. To aid this interpretation the spectral frequency axis is normalized to remove the effect of the individual patient heart rate. The frequency axis of all the PSDs are normalized by multiplying the frequency values by the threshold crossing mean value (sec). The amplitudes of the peak velocity variance, and the cardiac cycle mean velocity variance are normalized by the global mean cardiac cycle mean velocity (mm/sec)[2] (see Figures 45 and 46).

Figure 45

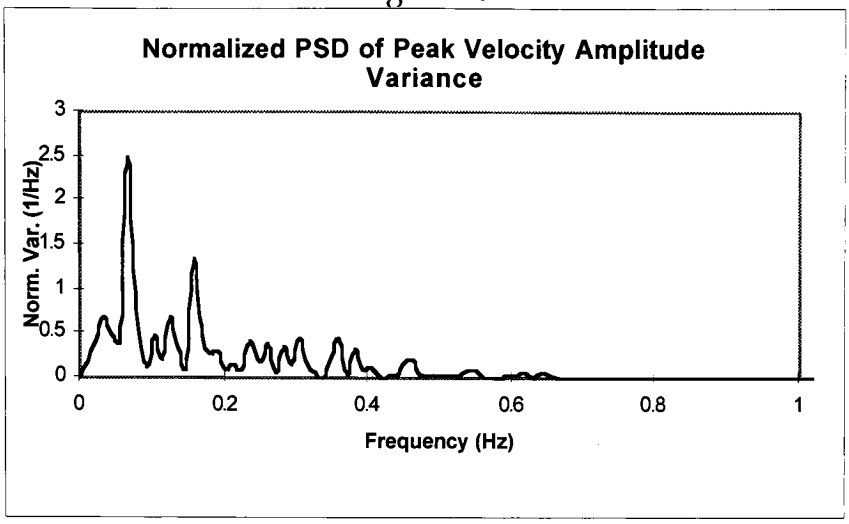

Figure 46

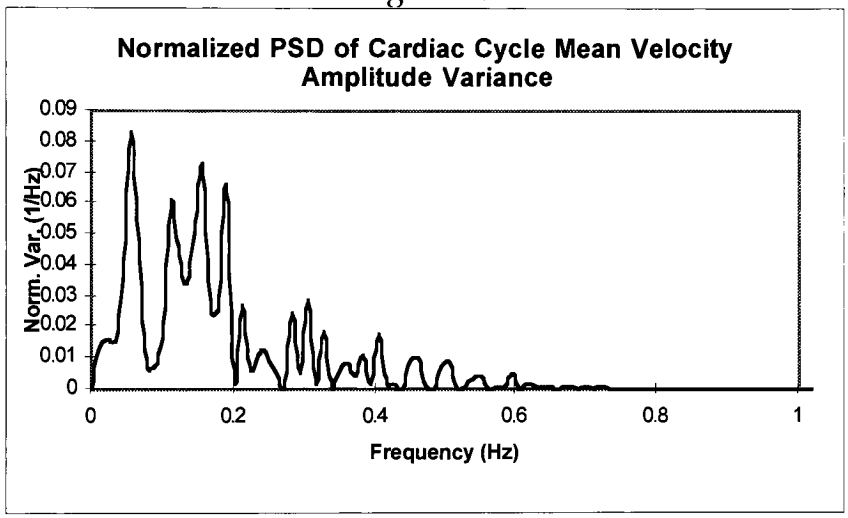

The periodicity PSDs amplitudes are normalized by dividing by the threshold crossing mean value $(sec)^2$ (see Figures 47 and 48).

Figure 47

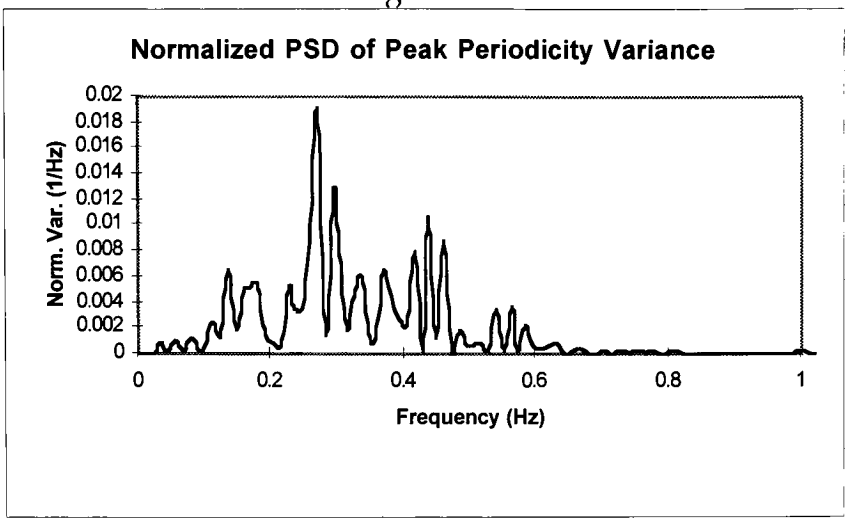

Figure 48

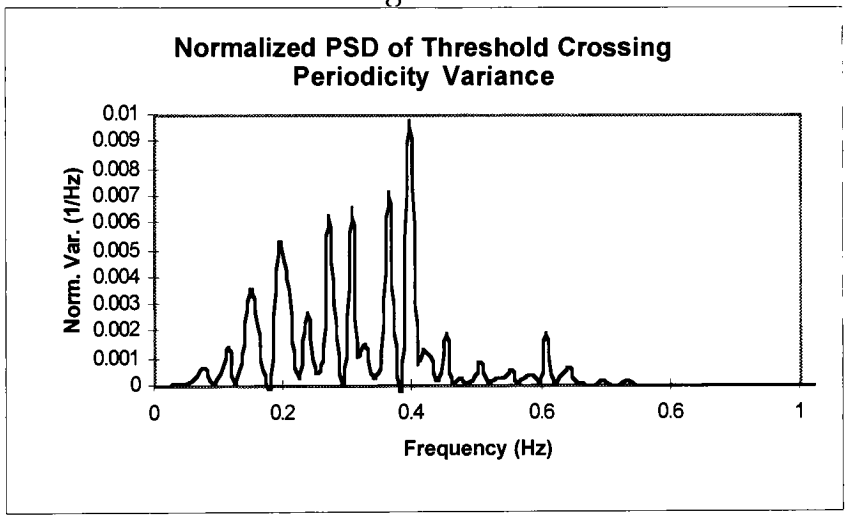

The Heart Rate PSDs are normalized by dividing the magnitudes by the heart rate threshold crossing $(BPM)^2$ (see Figures 49 and 50).

Figure 49

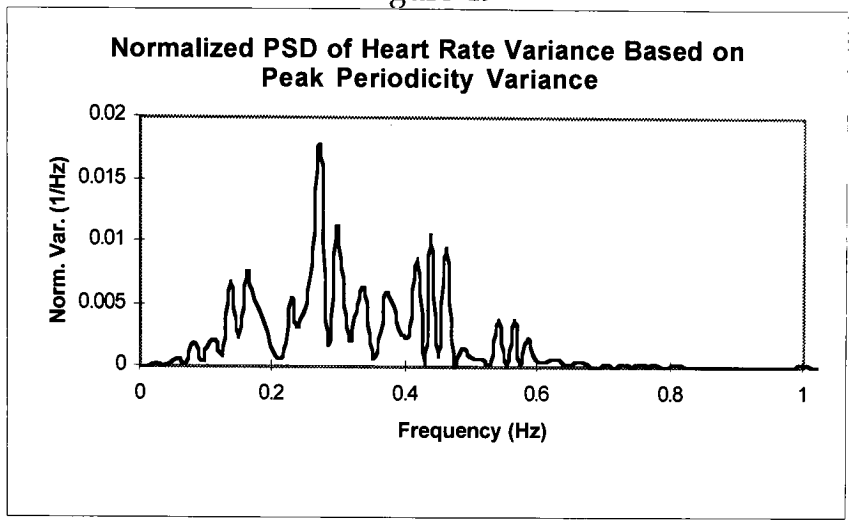

Figure 50

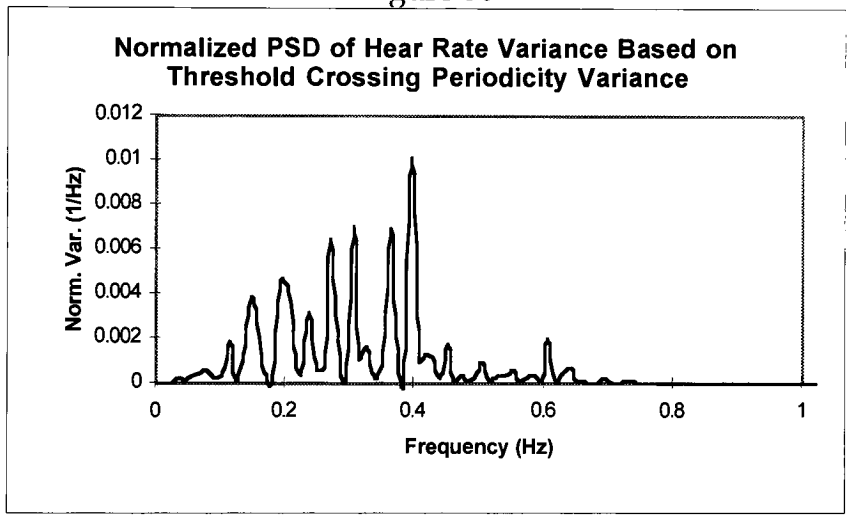

The normalized spectral data are saved to respective data files for further post-processing (not part of this thesis). The results of this post processing will ultimately allow us to define norms for fetal cardiovascular well being.

6 Discussion

Clinical cardiology and cardiovascular physiology involve the measurement of physical variables that are functions of time. These variables include heart rate, respiration rate, blood pressure, and blood flow. Each variable has its own characteristic waveform which reflects the pulsatile nature of cardiac mechanics and cardiovascular system response over an observed time interval. While much information can be obtained through descriptive hemodynamics [7, 14] additional details can be revealed through mathematical analysis. This is particularly true in light of the morphologic and functional changes that occur during development [31].

Primary morphogenesis occurs before the development of a functioning autonomic nervous system. In the chick peripheral adrenergic vascular receptors appear at stage 21, but are functionally inactive until after stage 29 [34]. Therefore, early development of the heart and circulation occurs without sympathetic and parasympathetic feedback mechanisms to monitor and regulate hemodynamics. This is in sharp contrast to the fetus and neonate where hemodynamic function is regulated by neural mechanisms manifest in heart rate variations [35, 36, 37, 38].

Heart rate variability [21] is an example of a frequency modulated hemodynamic signal indicative of neural control. The heart rate fluctuates with time about the mean heart rate on a time course spanning many seconds.

The nominal blood velocity waveform (or EKG) is the carrier signal, with fluctuations in cardiac cycle length (or Heart Rate) being the modulating signal.

6.1 Hemodynamic Control

Blood pressure and blood flow are regulated at cellular, tissue, organ, network, and neural levels. Previous studies of physiologic waveforms have yielded important information on cardiovascular function. Many physiologic waveforms of cardiovascular origin are pseudo-periodic in their time course [39]. Heart and respiration waveforms from healthy individuals may appear to be periodic for short durations. Fluctuations in periodicity are apparent however if hemodynamic waveforms are observed over longer durations. Heart rate variability was observed as early as 1733 by Hales [39] from periodicity variations in arterial blood pressure. Subsequent analyses of arterial pressure and electrocardiographic waveforms have revealed a close relationship between autonomic tone and the modulations in hemodynamic waveform periodicity [21].

Cardiovascular regulation in the preinnervated chick embryo is evident from alterations in cardiac afterload which encompass several cardiac cycles. Embryonic blood flow velocity [40] and vascular input impedance [18] are amplitude modulated. In the chick embryo peak-velocity amplitude modulation occurs (on average) every 13 cardiac cycles at Stage 21, every 18 cardiac cycles at Stage 18, and every 22 cardiac cycles at Stage 27. The change in

amplitude modulation periodicity from Stages 21 to 27 likely reflects shifts in hemodynamic control associated with morphogenesis.

The mature cardiovascular system is primarily regulated through neural control mechanisms. Cardiac output is controlled by variations in cardiac pacing and contractility, and vascular tone in response to autonomic neural activity and input from the renin-angiotensin system. Neural feedback occurs from respiratory sinus arrhythmia, baroreflex, and thermoregulation.

6.2 Interpretation and Speculation

The exact mechanism for afterload regulation in the preinnervated embryo is unknown. However, vascular input impedance modulation suggests biochemically mediated ventricular-vascular coupling. Candidate substances include atrial naturetic peptide [41], endothelium derived relaxation factor [42], and angiotensin [43]. Endothelium derived relaxation factor is a potent vasodilator and atrial naturetic peptide is a venodilator in the preinnervated embryo. These substances are abundant in the embryonic ventricle and can be secreted into the circulation thereby affecting vascular impedance. Indeed, vascular impedance shifts are documented in mature [44] and fetal [43] circulations during nitroprusside induced vasodilatation and angiotensin induced vasoconstriction.

The development of computational methods for the detection of heart rate variability and the analysis of its spectral content have defined various aspects of sympathetic and parasympathetic cardiovascular regulation in adults

[45, 46, 47], children [19, 36], and neonates [37, 38]. Heart rate variability has been studied in growth retarded fetuses from 38 to 41 weeks of gestation [35]. The arterial flow velocity waveforms of growth retarded fetuses have also been studied from 25 to 38 weeks [48]. However, the analysis of heart rate variability and flow velocity waveforms during early pregnancy has been elusive until now. The algorithms documented in this thesis provide computational tools to scrutinize blood velocity waveforms from 10 - 20 weeks gestation.

A fundamental change in hemodynamic regulation likely occurs from early to late in development; with heart rate (autonomic) control mechanisms appearing subsequent to flow amplitude modulation control. Pilot investigations in our laboratory [49] indicate both amplitude and frequency modulation of dorsal aortic blood velocities exist in the Stage 35 chick embryo, and human embryo-fetus at 12 weeks gestation. The results shown in section 5.3 corroborate the human fetal observations.

Hemodynamic regulation in the embryo-fetus therefore shifts from biochemical to neural mediation with cardiovascular development. This transition is of clinical importance since chronic shifts in the determinants of hemodynamic function have profound influence on cardiac morphogenesis [6].

6.3 Future Considerations

Although these preliminary results show promise in identification of fetal heart trends, it should be emphasized that further analysis will be necessary to validate the frequency domain results. Peaks in the spectra may not correlate to actual harmonics of the data, but instead may be related to the signal processing itself (see Appendix E).

References

1. Specialized Center of Research in Pediatric Cardiovascular Disease, SCOR Grant P50 HL51498, pp 200-201.

2. Marieb E : Human Anatomy and Physiology, Benjamin/Cummings Publishing Company, Inc., Redwood City, CA, 1995, pp 638-639.

3. Clark EB, Van Mierop L : Development of the Cardiovascular System, pg 2.

4. Clark EB: Cardiac Embryology, American Journal of Diseases of Children, 1986, pg 42.

5. Clark EB, Takao A, (eds) : Developmental Cardiology: Morphogenesis and Function, Mount Kisco, NY, Futura Publishing Co., Inc., 1990, pgs 5, 6.

6. Clark EB : Hemodynamic Control of the Embryonic Circulation, Developmental Cardiology: Morphogenesis and Function, Mount Kisco, NY, Futura Publishing Co., Inc., 1990, pg 299.

7. Broekhuizen M, Piet F, Struijk P, Van Der Bie W, Mulder p, Gittenberger-De Groot A, Wladimiroff J : Hemodynamic Parameters of Stage 20 to Stage 35 Chick Embryo, Pediatric Research, 1993, pg 46.

8. Kisslo J, Adams D, Mark D : Basic Doppler Echocardiography, New York, NY, Churchill Livingstone Inc., 1986, pgs 2, 9, 34.

9. Hein I, O'Brien W : A Flexible Blood Flow Phantom Capable of Independently Producing Constant and Pulsitile Flow with a Predictable Spatial Flow Profile for Ultrasound Flow Measurement Validations, IEEE Transactions on Biomedical Engineering, 1992, pg 1111.

10. Labovitz A : Doppler Echocardiography, Philadelphia, PA, Lea & Febiger, 1988, pg 1.

11. Jaffe C : Vascular and Doppler Ultrasound, New York, NY, Churchill Livingstone Inc., 1984, pg 18.

12. Piek J, Koolen J, Metting Van Rinj A, Bot H, Hoedemaker G, David G, Dunning A, Spaan J, Visser C : Spectral Analysis of Flow Velocity in the Contralateral Artery During Coronary Angioplasty : A New Method for Assessing Collateral Flow, JACC, 1993, pg 1525.

13. Kou T, Chan S : Continuous, on-line, Real Time Spectral Analysis of Systemic Arterial Pressure Signals, American Physiological Society, 1993, pg H2211.

14. Hu N, Clark EB, : Hemodynamics of the Stage 12 to Stage 29 Chick Embryo, Circulation Research, 1989, pg 1665.

15. Zahka K, Hu N, Brin K, Yin F, Clark EB : Aortic Impedance and Hydraulic Power in the Chick Embryo from Stages 18 to 29, Circulation Research, 1989, pg 1091.

16. Kempski MH, Matalevich J, Dzakowic J, Hu N, Clark EB : Cardiac Afterload Model of the Stage 21 Chick Embryo, pg 1.

17. Kaplan D, Talajic M : Dynamics of Heart Rate, American Institute of Physics, 1991, pg 252.

18. Kempski MH, Kibler N, Blackburn J, Dzakowic J, Hu N, Clark EB : Hemodynamic Regulation in the Chick Embryo, Bioengineering Conference ASME, 1993, pg 120.

19. Goldstein B, DeKing D, Delong D, Kempski MH, Cox C, Kelly M, Nichols D, Woolf P : Autonomic Cardiovascular State after Severe Brain Injury and Brain Death in Children, Critical Care Medicine, 1993, pg 229.

20. Goldstein B, Woolf P, DeKing D, Delong D, Cox C, Kempski MH : Heart Rate Power Spectrum Analysis and Plasma Catecholamine Levels after Postural Change and Cold Pressor Test, Pediatric Research, 1994, pg 359.

21. Van Ravenswaaij-Arts C, Kollee L, Hopman J, Stoelinga G, Van Geijn H : Heart Rate Variability, Annals of Internal Medicine, 1993, pg 438.

22. Peebles P : Probability, Random Variables, and Random Signal Principles 3rd ed., New York, NY, McGraw Hill Inc., 1993, pg 168.

23. Soliman S, Srinath M : Continuous and Discrete Signals and Systems, Englewood Cliffs, NJ, Prentice Hall, 1990, pgs 200, 203.

24. Press W, Flannery B, Tuekolsky S, Vetterling W : Numerical Recipes (FORTRAN), New York, NY, Cambridge University Press, 1989, pg 387.

25. Fahy K, Perez E : Fast Fourier Transforms and Power Spectra in LabVIEW, Application Note 40, National Instruments, 1993, pg 17.

26. Stremler F : Introduction to Communication Systems 3rd ed., Reading, MA, Addison Wesley Publishing Co., 1990, pg 137.

27. Strum R, Kirk D : Contemporary Linear Systems Using MATLAB, Boston, MA, PWS Publishing Co., 1994, pg 573.

28. Pickerd J : FFT Applications for TDS, Tektronix, 1993, pg 17.

29. Oppenheim A, Schafer R : Discrete Time Signal Processing, Englewood Cliffs, NJ, Prentice Hall, 1989, pgs 447, 590.

30. Hewlett Packard HP33120A Function Generator User's Guide, 1994, pg 41.

31. Kempski MH : Modeling and Control of Embryonic Hemodynamics, Developmental Mechanisms of Heart Disease, Armonk, NY, Futura Publishing Co., Inc., 1995, pg 426.

32. LabVIEW Analysis VI Reference Manual, National Instruments, 1994, Ch. 4, pg 11.

33. Panasonic AG-W1 VCR Operating Instructions, pg 33.

34. Pappano AJ, 1977, Ontogenic development of autonomic neuroeffector transmission and transmitter reactivity in embryonic and fetal hearts, Pharmacologic Reviews, 29:3-33.

35. Breborowicz G, Moczko J, Gadzinowski J 1988: Quantification of the fetal heart rate variability by spectral analysis in growth-retarded fetuses. Gynecol Obstet Invest 25:186-191.

36. Finley JP, Nugent ST, and Hellenbrand W 1987: Heart-rate variability in children: Spectral analysis of developmental changes between 5 and 24 years. Can J Physiol Pharmacol 65:2048-2052.

37. Kitney RI and Rompelman O 1987: Heart rate variability in neonates. in The Beat-by-Beat Investigation of Cardiovascular Function, Kitney RI and Rompleman O, eds. Oxford, UK, Clarendon Press.

38. Siimes ASI, Valimaki IAT, Antila KJ, Julkunen MKA, Metsala TH, Halkola LT, and Sarajas HSS 1990: Regulation of heart rate variation by the autonomic nervous system in neonatel lambs., Pediatr Res 27:383-391.

39. Baselli G, Cerutti S, Civardi S, Lombardi D, Malliani A, Merri M, Pagani M, and Rizzo G 1987: Heart rate variability signal processing: a quantitative

approach as an aid to diagnosis in cardiovascular pathologies. Int J Bio-Med Comp 20:51-70.

40. Kempski MH, Blackburn JL, Hu N, and Clark EB, 1992, Power Spectrum Analysis of Dorsal Aortic Blood Velocity in the Stage 21, 24 and 27 Chick Embryo, Pediatric Res., 31(4)20A.

41. Nakazawa M, Kajio F, Ikeda K, and Takao A, 1990, Effect of atrial natriurtic peptide on hemodynamics if the stage 21 chick embryo, Pediatric Res., 27(6):557-560.

42. Ohyanagi M, Nishigaki K, and Faber JE, 1992, Interaction between microvascular a_1- and a_2-adrenoceptors and endothelium-derived relaxing factor, Circulation Res., 71:188-200.

43. Adamson SL, Whiteley KJ, and Langille BL, 1992, Pulsatile pressure-flow relations and pulse-wave propagation in the umbilical circulation of fetal sheep, Circulation Res., 70:761-772.

44. Yin FCP, Guzman PA, Brin KP, Maughan WL, Brinker JA, Traill TA, Weiss JL, and Weisfeldt ML, 1983, Effect of Nitroprusside on Hydraulic vascular loads

on the right and left ventricle of patients with heart failure, Circulation, 67(6):1330-1339.

45. Akselrod S, Gordon D, Madwed JB, Snidman JC, Shannon DC, and Cohen RJ 1985: Hemodynamic regulation: investigation by spectral analysis. Am J Physiol 249:H867-H875.

46. Kitney RI and Rompelman O 1980: The Study of Heart-Rate Variability. Oxford, Clarendon Press.

47. Saul JP, Berger RD, Albrecht P, Stein SP, Chen MH, and Cohen RJ, 1991, Transfer function analysis of the circulatio: unique insights into cardiovascular regulation, Am J Physiol. 261 (Heart Circ. Physiol. 30): H1231-1245.

48. Groenenberg IAL, Wladimroff JW, and Hp WCJ, 1989, Fetal cardiac and peripheral arterial flow velocity waveforms in intrauterine growth retardation, Circulation, 80:1711-1717.

49. Kempski MH, Broekhuizen MLA, Wladimiroff JW, and Clark EB, 1994, unpublished observations.

Appendix A

Audio Frequency Response of the Panasonic AG-W1 VCR

The following procedure was used to determine the Hi-Fi audio frequency response characteristics of the AG-W1 VCR:

1) An HP 33120A function generator (output: high impedance) was used to generate a sine wave having an amplitude of 1 Vp-p, and frequencies of 1, 2, 5, 10, 20, 50, 100, 200, 500, 1k, 2k, 5k, 10k, 20k and 40k (Hz). The output from the function generator was connected to the right channel (R) of Audio In Line 1 on the AG-W1 VCR. The output from the function generator was also connected to the HP54602A oscilloscope.

2) A blank tape (3M T-60 Broadcast video cassette) was inserted into the AG-W1 VCR, and each of the waveforms mentioned above were recorded (for a duration of one minute) onto the tape. While the VCR was recording the waveform (from the function generator), the amplitude and frequency of this waveform was measured using the oscilloscope. These measurements appear in Table A-1, columns A and B.

3) The tape was then played back. The output (from audio output (R) of line 1) was routed to the HP 54602A oscilloscope. The amplitude and frequency of the output signals from the tape were measured using the oscilloscope. These measurements appear in Table A-1, columns C and D.

The data in Table A-1 is organized in the following way: column A presents the amplitudes of the sine waves which were recorded onto the tape (input), at the respective frequencies shown in column B. Column C presents the amplitudes of the sine waves as measured when the tape was played back (output), at the frequencies noted in column D. Column E presents the respective amplitude ratios (output/input) in dB. The equation used to determine the amplitude ratio was:

$$\mathbf{AR(dB) = 20 \cdot \log_{10}\left(\frac{V_{pp\ tape}}{V_{pp\ in}}\right)} \qquad \text{(A 1.1)}$$

The data obtained from this test was used to construct a Bode Diagram shown in Figure A-1. The results obtained from this test are consistent with the frequency range (20 Hz to 20 kHz) for this unit. (See Hi-Fi sound Specifications (page 33 (enclosed)).

Table A-1

A	B	C	D	E
Vpp in (V)	fscope (Hz)	Vpp tape (V)	ftape (Hz)	AR (dB)
1.062	1	0.33	1	-10.28
1.062	2	0.72	2	-3.39
1.062	5	1.13	5	0.50
1.062	10	1.25	10	1.42
1.062	20	1.28	20	1.63
1.062	50	1.30	50	1.74
1.062	100	1.30	100	1.74
1.062	200	1.30	200	1.74
1.062	500	1.30	500	1.74
1.062	1000	1.30	1000	1.74
1.062	2000	1.30	2000	1.74
1.062	5000	1.30	5000	1.74
1.062	10000	1.30	10000	1.74
1.062	20000	1.22	20000	1.20
1.062	40000	0.31	40000	-10.63

Figure A-1

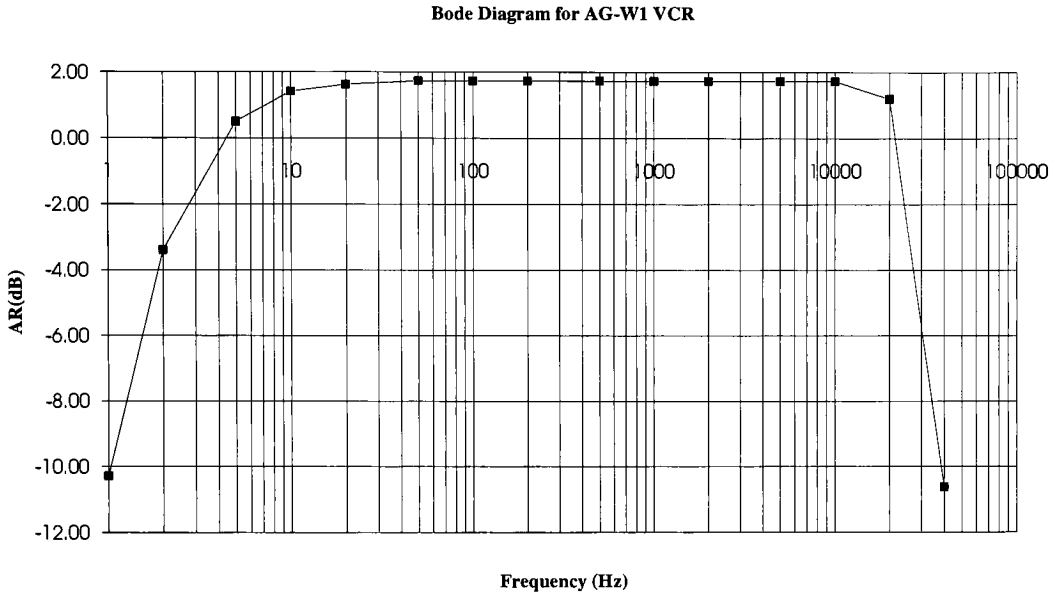

In order to determine the dual channel recording capabilities of the Panasonic AG-W1 VCR, a sweep sine test was performed. The testing was conducted using the procedure outlined below:

1) An HP 33120A function generator (output: high impedance) was used to generate a sine wave having an amplitude of 1 Vp-p, an frequencies of 2, 20, 200, 2k, 20k (Hz). The output from the function generator was connected to the right channel (R) of Audio In Line 1 on the AG-W1 VCR.

2) A blank tape was inserted into the AG-W1 VCR, and each of the waveforms mentioned above were recorded (for a duration of three minutes) onto the tape.

3) The tape was then played back. The output (from audio output (R) of line 1) was routed to the HP 54602A oscilloscope. The oscilloscope then performed the FFT (Fast Fourier Transform) on the output from the VCR. The waveforms which were recorded on the Right channel of Audio In Line 1 (along with the FFT) are shown in Figures A-2 through A-6.

4) The output from the function generator was then routed to the Left channel (L) of Audio In Line 1, and steps 1, 2, 3 were repeated. The waveforms which were recorded on the Right channel (R) of Audio In Line 1 (along with the FFT) are shown in Figures A-7 through A-11. The data indicate no L/R bias between recording channels and that each channel conforms to the manufacture's specifications.

Note Figures A-2 and A-7 show an output which is periodic, but not representative of the input sine wave. This may be a consequence of the AG-W1 pass-band frequency range of 20 Hz to 20 kHz, such that the 2 Hz signal of Figures A-2 and A-7 is distorted. Also note that there is a harmonic associated with the 20 kHz output signal from the VCR (see Figures A-6 and A-11).

Published information pertaining to the frequency range of the AG-W1 was obtained from the Operators Instructions manual. See Hi-Fi sound Specifications (page 33 (enclosed)).

HP Benchlink software was used to transfer the images shown in Figures A-2 through A-11 from the oscilloscope into this document.

Figure A-2

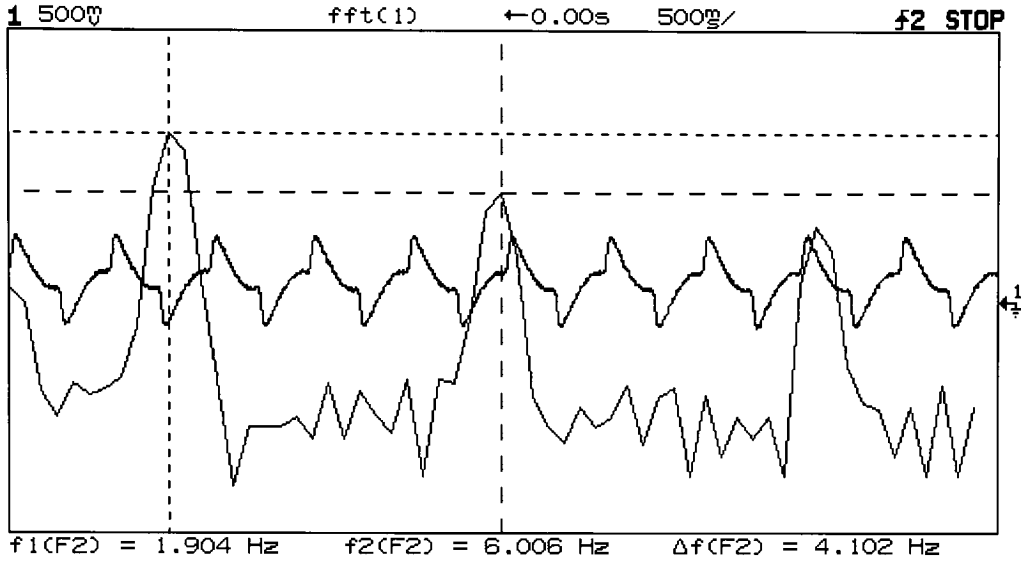

Figure A-3

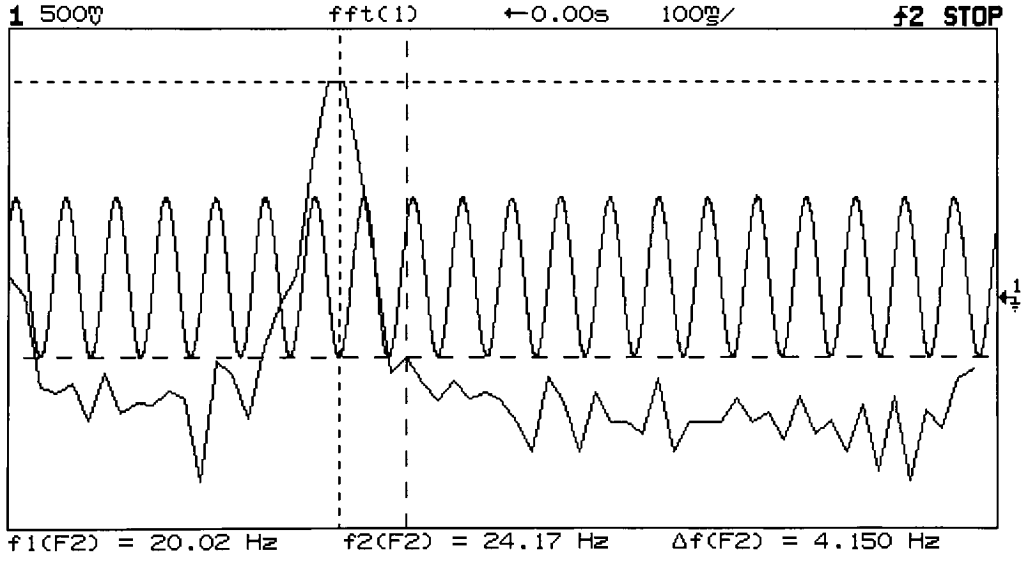

Figure A-4

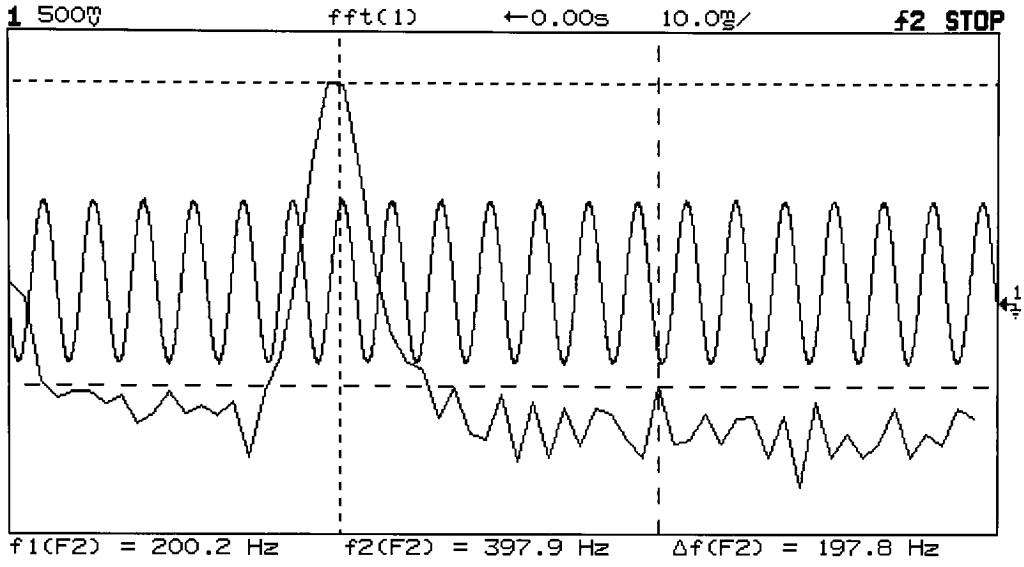

Figure A-5

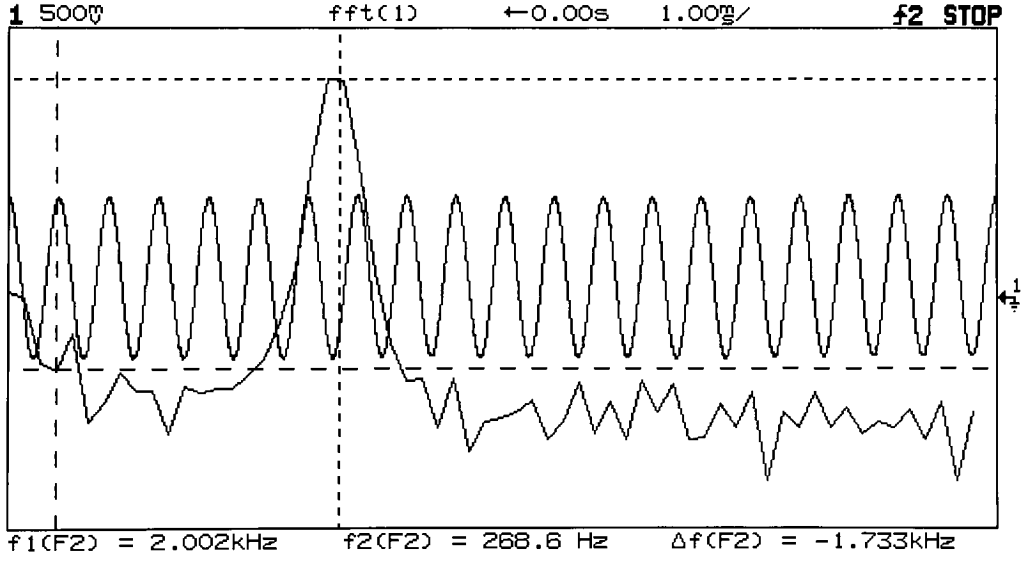

Figure A-6

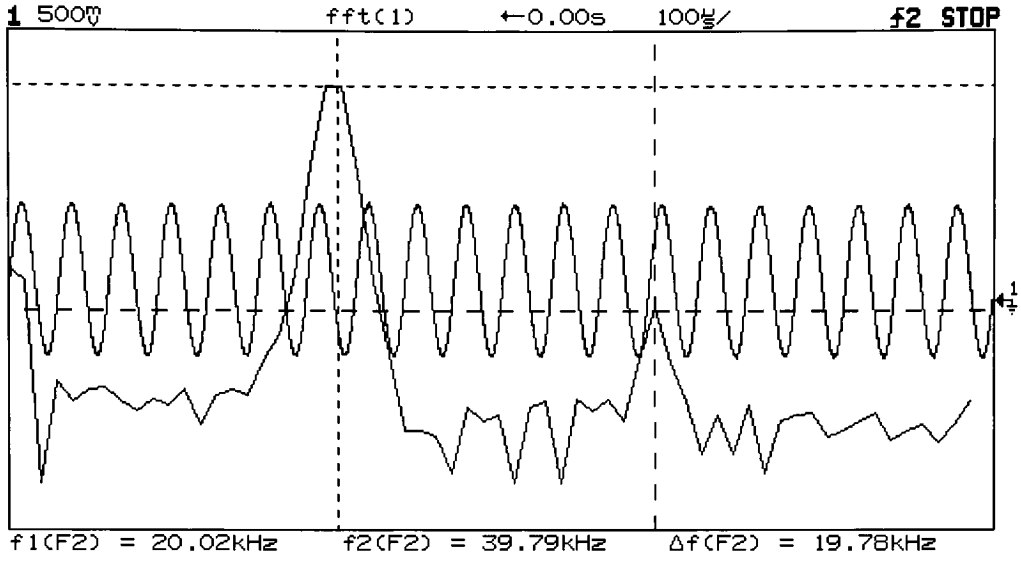

peak1=-9.043dBV, peak2=-44.69dBV (dBV referenced to 1 Vrms)

Figure A-7

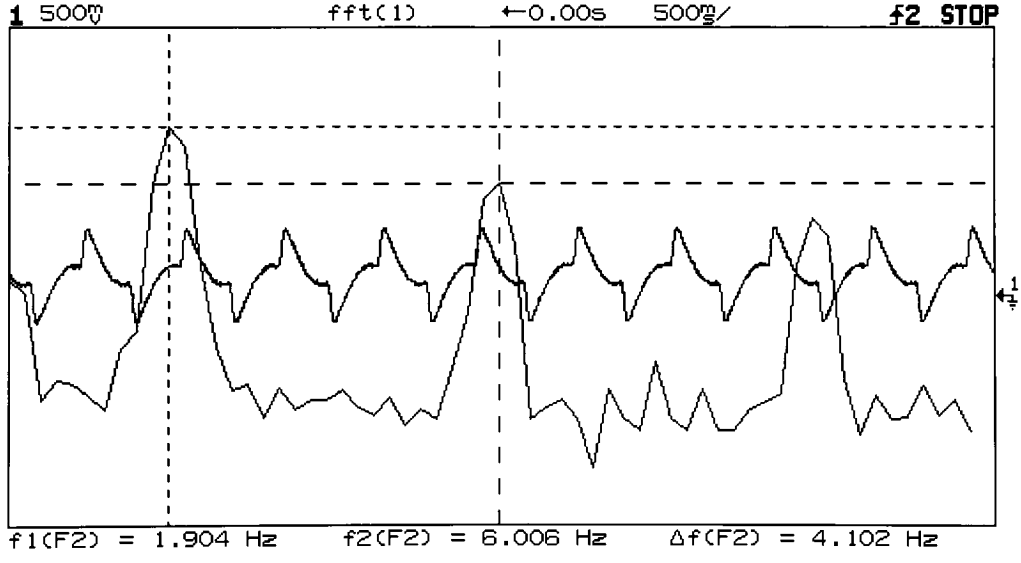

Figure A-8

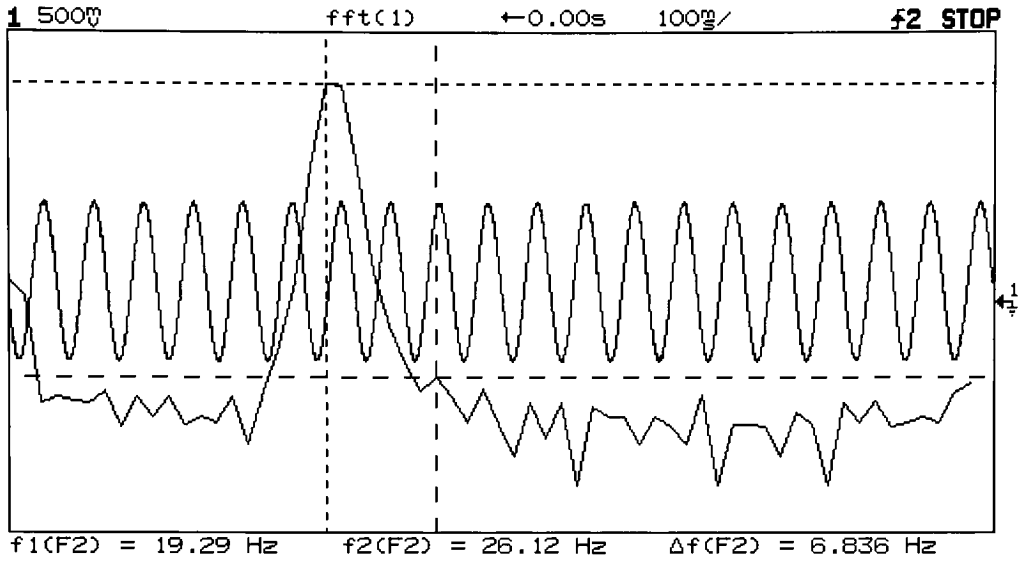

Figure A-9

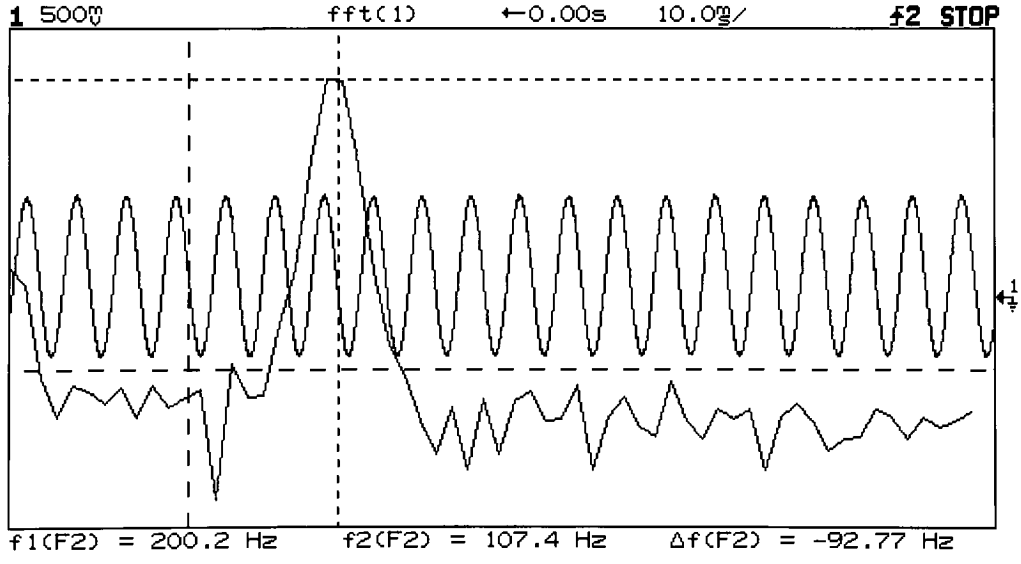

Figure A-10

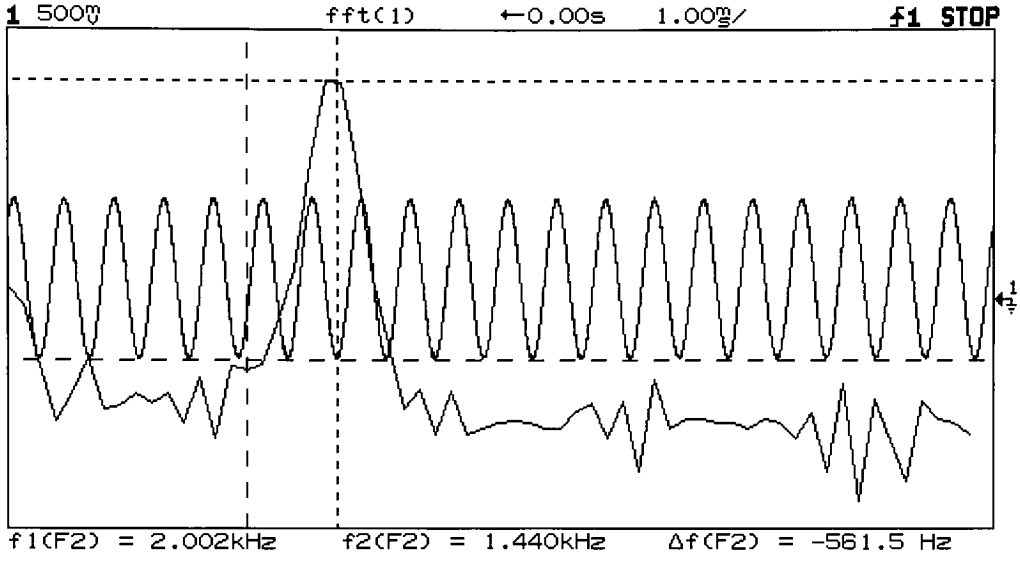

Figure A-11

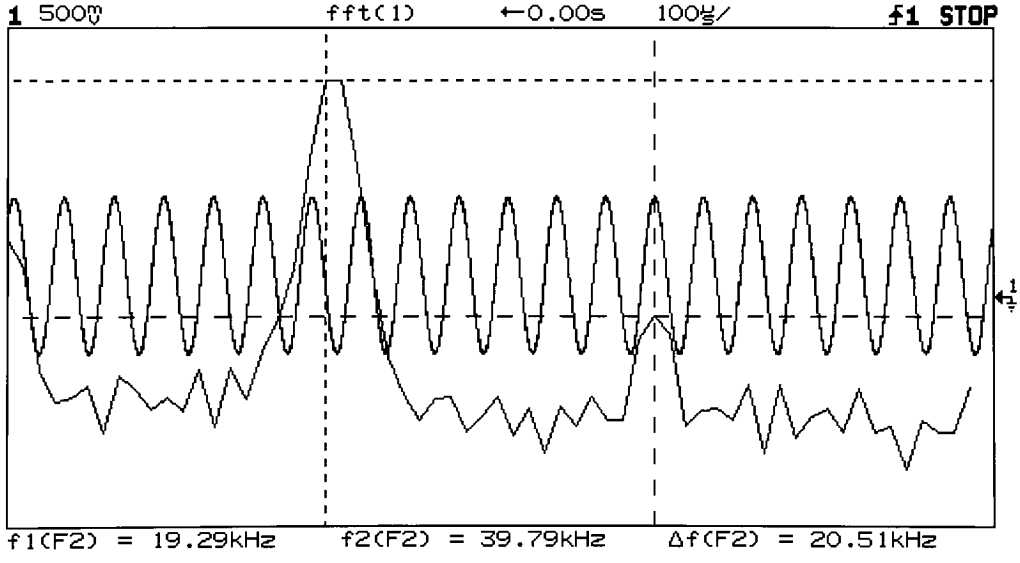

v1=-8.7dBV v2=-46.25dBV (dBV referenced to 1 Vrms)

Table A-2 displays the specifications for the Panasonic AG-W1 VCR [33].

Table A-2

SPECIFICATIONS

is the safety information

Power Source:		AC 110~127/220~240 V±10%, 50/60 Hz±0.5%		
Power Consumption:		Approx. 42 watts (8 watts when turned off)		
Video Recording System:		2 rotary heads, azimuth recording system, VHS standard		
TV System:		NTSC/M-PAL 525 lines/60 fields	PAL/N-PAL 625 lines/50 fields	SECAM 625 lines/50 fields
Tape Speed:		SP: 33.35 mm/sec. SLP: 11.12 mm/sec.	SP: 23.39 mm/sec. LP: 11.7 mm/sec	SP: 23.39 mm/sec. LP: 11.7 mm/sec.
Tape Format:		12.7 mm wide high density video tape (½") VHS video cassette (with easy playback function for S-VHS cassettes)		
Record/Playback Time:		Maximum 8 h. with NV-T160	Maximum 8 h. with NV-E240	Maximum 8 h. with NV-E240
FF/REW Time:		Less than 5½ min. with NV-T120/NV-E180		
Modulation System:	**Luminance:** **Color signal:**	FM azimuth recording converted subcarrier phase shift recording	FM azimuth recording converted subcarrier phase shift recording	FM azimuth recording ¼ countdown
Input Level: (Pin Jack)		1.0 Vp-p, 75 ohm		
Output Level: (Pin Jack)		1.0 Vp-p, 75 ohm		
Audio Input Line:		−10 dBV, more than 50 kohm		
Audio Line Output:		−8 dBV, less than 1 kohm		
Headphone:		8Ω		
Audio Track:		Hi-Fi stereo; 2 channels, Normal mono; 1 track		
Hi-Fi Sound Specifications:		Dynamic Range; more than 90 dB, Frequency Range; 20 Hz~20 kHz Wow & Flutter; less than 0.005%		
Dimensions:		18⁹⁄₁₆" (W)×4⁹⁄₁₆ (H)×15½ (D) [464 (W)×105.5 (H)×392.5 (D) mm]		
Weight:		Approx. 18¹⁄₁₆ lbs (8.2 kg)		
Operating Temperature:		5°C~40°C		
Operating Humidity:		35%~80%		
Special Playback Speeds:		Speed Search: NTSC/M-PAL about 11× (in SP mode 5×) PAL/N-PAL/SECAM/MESECAM approx. 9× (in SP mode 7×) noise lock Slow : ¹⁄₃₀~⅛×		

Appendix B

Calibration of the Lab PC+ Data Acquisition Board

The following procedures were used to calibrate the National Instruments Lab PC+ data acquisition board to a DC input and a harmonic input:

1) A constant DC voltage was supplied to the Lab PC + data acquisition board using the TEK CPS 250 power supply. The input voltage to the board was measured on a TEK CDM 250 digital multimeter. The voltage the board received was measured using a test VI in LabVIEW.

2) A sine wave having a fixed amplitude and varying frequency was supplied to the Lab PC+ data acquisition board using a Wavetek 182 A function generator. The peak to peak amplitude, and frequency of the input waveform was measured on a TEK 2221 oscilloscope. The peak to peak amplitude and frequency of the waveform the board received was measured using a test VI in LabVIEW.

The data obtained from the DC calibration is shown in Table B-1. The data obtained from the harmonic calibration is contained in Table B-2.

Figure B-1 shows the calibration curve for the data acquisition board using a DC input voltage. The DC voltage measured using LabVIEW is displayed on the vertical axis. The DC voltage measured using the TEK CDM

250 multimeter is displayed on the horizontal axis. The slope of this line is 1.0018.

Figure B-2 shows the calibration curve for the data acquisition board using a harmonic input. The frequency measured using LabVIEW is displayed on the vertical axis. The frequency measured using the TEK 2221 oscilloscope is displayed on the horizontal axis. The slope of the line is .99849. We conclude that the board is working properly.

Data Acquisition Board Calibration Data

Table B-1

Vi (V) TEK	Vi (V) LV
0.489	0.486
0.740	0.740
0.989	0.984
1.238	1.238
1.496	1.492
1.988	1.980
2.990	2.986
3.980	3.980
4.500	4.497
4.980	4.978

Slope= 1.00018887

Table B-2

TEK Oscilloscope		Lab VIEW			
Vi (V)	f (Hz)	f (Hz)	Vi (V)	% err. Vi	% err. f
1.04	0.06688	0.06724	1.0523	1.18	0.54
1.04	0.2127	0.2186	1.0547	1.41	2.77
1.04	3.333	3.33	1.0376	0.23	0.09
1.04	33.33	33.33	1.0340	0.58	0.00
1.04	333.3	333.3	1.0351	0.47	0.00
1.04	2000	2000	0.9863	5.16	0.00
1.04	3257	3333	1.0376	0.23	2.33
1.04	11420	11428	1.0547	1.41	0.07

Slope= 0.99848952

Figure B-1

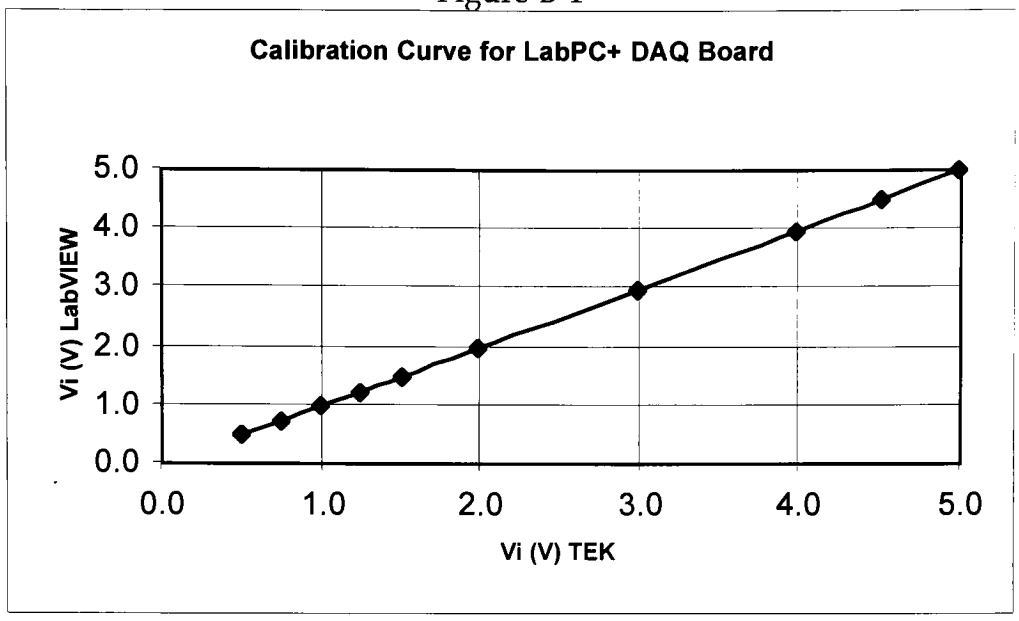

Figure B-2

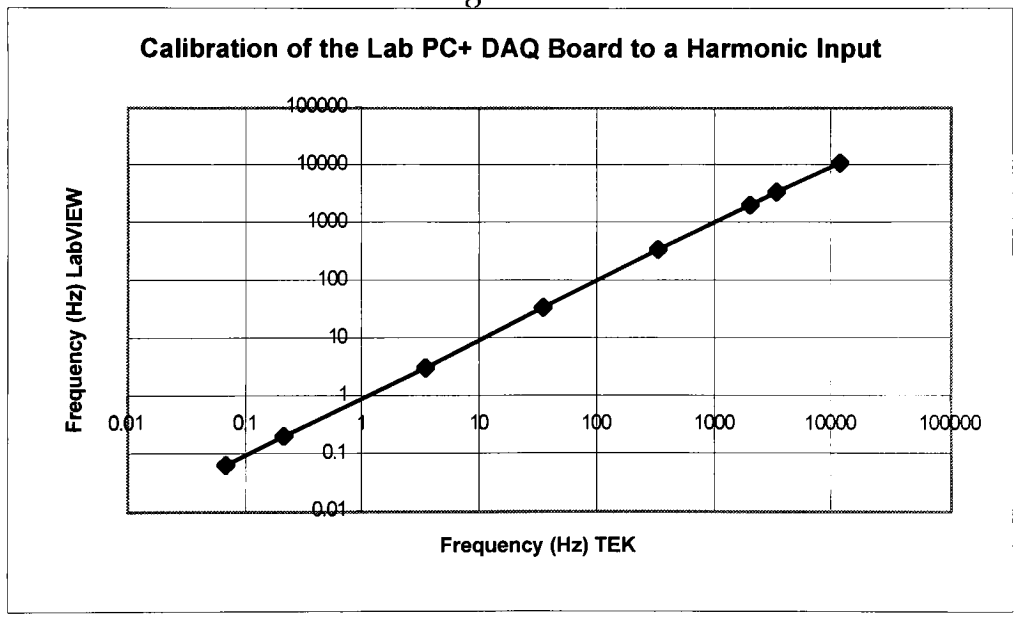

Appendix C

Glossary and Description of User Controls

Main Control: Allows the user to acquire data, process data, analyze data or exit the program.

C.1 Acquisition Parameters

Acquire Data From: Specifies the data acquisition channel (Audio Channel Left: Ch 0, Audio Channel Right: Ch 1, Dual Channel Acquisition: 0,1).

Acquire N Seconds of Data: Specifies how many seconds of data to acquire.

C.2 Processing Parameters

Percent Overlap: The overlap is specified as a percentage. The percent overlap and the number of scans to read from the file determine how far back the file marker indicator will move. (50 % overlap default).

Number of Scans to Read at a Time: The number of scans read from the file during each loop iteration. If the number of scans read from the file is not a power of two error trapping will change the value so that it becomes a power

of two. This is necessary because the data packet is run through an Fast Fourier Transform (FFT), and if the packet size is not a power of two, the Discrete Fourier Transform (DFT) will be used instead and this is undesirable because the DFT is very computational intensive. (1024 default).

Probe Type: The probe type is either a transabdominal probe, or a transvaginal probe. The frequency associated with the transabdominal probe is 5 MHz, the frequency associated with the transvaginal probe is 6 MHz. The transducer frequency is used in scaling frequency values to velocity values via the Doppler equation.

Butterworth Filter Type: Allows the user to select a low pass filter, high pass filter, band pass filter, or band stop filter. (Low Pass Filter default).

Window: Allows the user to window the velocity data prior to spectral analysis. (No Window default).

Filter Order: Specifies the order of the Butterworth filter. (5th order).

Cutoff Frequency: Cutoff Frequency of the Butterworth filter. (4 Hz default).

Invert Data?: This control will scale the data by negative one (-1) if for some reason the data is inverted (resulting from a dual channel acquisition). (Do not invert default).

Zero Padding: Pads the velocity time series with trailing zeros in order to enhance resolution in the frequency domain. (Pad twice default).

Set Intensity Threshold (dB): The user set a threshold for the intensity of the spectrum in the frequency domain. If the largest peak in the frequency spectrum is greater than the threshold value, the index at which this peak occurs is passed to the peak frequency array. If the largest peak in the frequency domain is less than the threshold value a zero is passed to the peak frequency array. (-70 dB default).

C.3 Analysis Parameters

Directory: Allows the user to specify a file path in which the spectral data will be stored.

Save Normalized Data to File: The program will automatically save the normalized spectra to a file. (Default Do Not Save).

Save Spectral Data to File: The program will automatically save the non-normalized spectra to a file. (Default Do Not Save).

Save Time Data to File: The program will automatically save the time series to a file. (Default Do Not Save).

Width: This control allows the user to set the width that defines how many points make up a valid peak.

Window: Allows the user to window the velocity data prior to spectral analysis. (No Window default).

Number of Interpolations: Performs the specified number of interpolations on the selected data sets.

Threshold: The threshold value is a percentage of the global mean. Setting a threshold allows the Threshold peak detection algorithm to peak detection.

Butterworth Filter Type: Allows the user to select a low pass filter, high pass filter, band pass filter, or band stop filter. (Low Pass Filter default).

Filter Order: Specifies the order of the Butterworth filter. (5th order).

Cutoff Frequency: Cutoff Frequency of the Butterworth filter. (4 Hz default).

Invert Data?: This control will scale the data by negative one (-1) if for some reason the data is inverted (resulting from a dual channel acquisition). (Do not invert default).

Zero Padding: Pads the velocity time series with trailing zeros in order to enhance resolution in the frequency domain. (Pad twice default).

Median Filter Rank: Allows the user to specify the rank of the median filter. (Default none).

Spectrum Type: Allows the user to select between an amplitude spectrum, or a power spectral density. (Default Power Spectral Density).

Detrend: The user specifies either linear, quadratic, or cubic. The detrending algorithm will then determine the best fit to the time series using a polynomial approximation whose order is specified by the user. (Default Quadratic).

Algorithm: Detrending algorithm. (Default SVD).

C.4 ASCII conversion to Velocity

Number of Data Columns: Number of data columns in the ASCII file.

Header Count: ASCII file header information (this header is striped from the file).

User Header: Displays the file header.

Velocity Scale Factor: Scales ASCII voltage data to velocity (mm/sec).

Velocity Column: Column in the ASCII data file that contains the velocity (voltage) data.

Time Column: Column in the ASCII file that contains the time data.

Time Sampling Unit: Converts seconds data from sec to sec.

Filter: The user can filter the velocity data using a Butterworth low pass filter. The user also has the option of not filtering the data.

Filter Order: Specifies the order of the Butterworth filter.

Cutoff Frequency: Cutoff Frequency of the Butterworth filter. If a low pass filter is used, the user must specify the a single cutoff frequency. If a bandpass filter is employed, the user must specify a low cutoff frequency, and a high cutoff frequency.

Appendix D

Program Descriptions

D.1 Description of *Chicken 2.VI*

It is assumed that the user has prior knowledge of the file format (how many columns of data are in the file, the number of lines in the header, etc.). Upon execution the VI will prompt the user for the name of an ASCII data file to read. The user chooses an ASCII data file, and then specifies a filename in which to store the velocity and time data.

First the VI opens the ASCII data file selected by the user. A sub VI (*Read ASCII Data File.VI*) strips the header and reads the ASCII data file. The data read from the file is stored in a 2-D array. The 2-D array is reshaped to a 1-D array. The 1-D array contains both the voltage and time data (interleaved).

Next the sub VI (*Scale ASCII to Time Velocity.VI*) takes the interleaved 1-D array, and creates two separate arrays (a voltage array, and a time array). The values in the time array are converted from msec to sec, and the values in the voltage array are converted into velocity (mm/sec). The velocity array is then passed into a case structure where it can be low pass filtered (provided the user wants to filter the data). If the user chooses to filter the data, a 5th order low pass Butterworth filter with a cutoff frequency of 15 Hz will be used by default.

Finally the size of the velocity array is determined, and the first two elements in the time array are extracted. The first two values in the time array

will be used to calculate dt. The size of the velocity array, the values t(0) and t(1) as well as the velocity array are saved to a file.

D.2 Description of the Acquisition Portion of *Main III.VI*

D.2.1 Acquisition:

To acquire human Doppler velocity data the user must specify the VCR audio channel they want to acquire data from (Audio Left, Audio Right, or dual channel), and the duration of the acquisition (sec). This is done in the acquisition parameters menu. The channel and duration are passed to a sub VI (*Get Acquisition Parameters.VI*)

The *Get Acquisition Parameters.VI* determines the sampling rate (based on channel selection) , the buffer size, and the number of scans to acquire. The sampling rate is 44 kHz for single channel acquisition, and 30 kHz for dual channel acquisition. The information is passed out of *Get Acquisition Parameters.VI* in to another sub VI (*Continuous Acquisition to File (binary).VI.* This VI prompts the user for a filename in which to store the data. This VI also interfaces with the data acquisition hardware to sample the input, and store these samples to a binary file.

D.2.2 Demodulation:

To demodulate the human data, and convert the frequency information into a velocity profile we must use the VI *Phase II.VI. Phase II.VI* demodulates

the sampled FM audio data, reconstructs the velocity profile, and stores this information to a data file.

First the VI prompts the user for a binary file. The user chooses the binary file, then specifies a file in which to store the reconstructed velocity profile. The VI then opens the binary file and strips the header. The header contains group channel settings (a cluster that is used to convert the binary data to 'scaled voltage data'), the sampling rate, the channel list, the number of channels in the file, and the user header. All of the header information is passed to a **while** loop.

Once inside the **while** loop N (N is a power of two) number of scans are read from the binary file. These scans are scaled from binary to 'scaled voltage data'. The scaled voltage data is passed into a case structure. If the file contains one channel of data, then the single channel is demodulated. If the file contains two channels of data, then both channels are demodulated. This demodulation is carried out in the sub VI *Process 2 with Pad.VI.*

The scaled voltage data is passed into *Process 2 with Pad.VI*, along with the user specified Intensity Threshold (used to reject low intensity peaks in the spectrum), window type, the time differential value dt, and the number of zero pads to perform.

Once in *Process 2 with Pad.VI*, the scaled voltage array is padded with zeros (up to two zero pads are performed). Padding the scaled voltage array with zeros gives us a larger array (up to four times the original size). As a

result of the zero padding the value of df will be smaller than it would have been had we not padded. The smaller value of df 'increases' the resolution in the frequency spectrum. If a window is selected, the data will be windowed.

Next, the power spectrum of the scaled voltage array is calculated using the LabVIEW *Auto Power Spectrum.VI*. The amplitude values returned from the Auto Power Spectrum are converted to dB (from V^2 rms). A max/min function (LabVIEW library routine) determines the maximum peak in the frequency spectrum, and the index at which this peak occurs. The magnitude of the largest peak is compared to the user specified intensity threshold. If the peak amplitude is larger than the intensity threshold value, then the index at which the largest peak occurred at is passed to the peak frequency index array. If the value of the intensity threshold is larger than the maximum peak value, a value of zero is passed to the peak frequency array. The value of df (determined from the Auto Power Spectrum) is also passed out of the *Process 2 with Pad.VI*. The values contained in the peak frequency and df arrays will be used to reconstruct the velocity profile. This completes one iteration of the loop. N number of scans are read from the file (with appropriate overlap), and the process outlined above repeats until the end of file is reached. Once the end of file is reached, the arrays containing the peak frequency indices, the values of df, dt, the number of scans to read, and the file read marker are passed into the sub VI *meanandlean.VI*. The *meanandlean.VI* reconstructs the frequency vs time profile. Subsequently the frequency array is scaled by the Doppler equation to obtain

velocity. The last value contained in the arrays passed to the sub VI *meanandlean.VI* are removed, because these values are erroneous due to reading the end of file marker.

A three packet averaging scheme will be employed to represent the average frequency of three data packets. We want the time at which the average frequency occurs to coincide with the midpoint of the absolute time of these data packets as they were contained in the binary file. To reconstruct the time series the scan index array, the number of scans to read array, and the dt array are needed. The average time is determined by the relation:

$$t_{ave} = \frac{(x(i+2) + x(i) - (\#\ \text{to read}))dt}{2} \qquad \text{(D-1)}$$

for any overlap. X(i) is the file marker indicator, # to read is the number of scans to read from the file, and dt is the time between two consecutive frequency values. The average frequency is determined by multiplying the indices at which the largest peak in the frequency spectrum occurred by the value of df. The mean value of three consecutive frequency values is determined and represents the three packet average frequency.

The frequency array is passed to the *Doppler Conversion to Velocity.VI*. This VI scales the frequency values by the Doppler equation to obtain velocity in (mm/sec). The Doppler Equation is:

$$V = \frac{1000 \cdot c \cdot f}{2 \cdot f_T \cdot \cos\theta} \qquad \text{(D-2)}$$

where c is the speed of sound in tissue, f is the three packet average frequency, f_T is the frequency of the transducer, and θ is the inclusive angle the probe makes with the blood flow.

The scaled velocity data is passed through a 5th order Butterworth low pass filter (default cutoff frequency=15Hz). This filter removes any high frequency velocity components. Finally the size of the velocity array is determined, and the first two elements in the time array are extracted. The first two values in the time array will be used to calculate dt. The size of the velocity array, the values t(0) and t(1) as well as the velocity array are saved to a file.

D.2.3 Analysis:

To analyze the velocity data, either from the human fetus, or the chicken embryos, the *Processed Chicken III.VI*, and its sub VI's must be called. When *Processed Chicken III.VI* executes control passes to a sub VI *Step 1.VI*. This VI prompts the user to select a file to be processed. *Step 1.VI* opens the file selected by the user, and reads the first three elements in the file (the velocity array size, the value of t(0), and the value of t(1)). Next the entire velocity array is read. *Step 1.VI* then computes the global mean value of the velocity time series, calculates dt, and reconstructs the time array. The parameters mentioned above are passed to *Step 2.VI*.

Step 2.VI uses the user specified value of percent of mean value to establish a threshold. The LabVIEW VI *Threshold Peak Detector.VI* determines the indices at which the rising edge of the velocity profile crosses the threshold

level. The threshold indices array is used to do peak detection. By inserting a max/min function in a 'for next' loop the maximum value of the velocity array between two consecutive threshold crossings, and the values at which it occurs are determined. These values represent the peak amplitudes and peak times, respectively. *Step 2.VI* passes the following parameters to *Step 3.VI*: threshold crossing index array, peak velocity values, peak velocity index, threshold level, dt, velocity, time and the global mean velocity value.

Step 3.VI uses the parameters passed to it to calculate the times at which peaks and threshold crossings occur, and the mean velocity per pulse. The times at which the peaks occur are determined by multiplying the peak index array by dt, and then adding t(0). The times a which the threshold crossings occur is found by using linear interpolation:

$$t_{th} = [\frac{V_{th} - V_{i-1}}{V_i - V_{i-1}} + (i_{th} - 1)] \cdot dt + t_0 \qquad \text{(D-3)}$$

The mean velocity per pulse is determined by creating a Sub array containing all the elements in the velocity array (between two consecutive threshold crossing indices) and computing the mean value of this Sub array.

Step 3.VI contains four arrays that are of interest to us. These arrays are the peak times, threshold times, mean pulse velocity, and the peak velocity amplitude arrays, respectively. These four data sets are passed into an interpolation algorithm which performs a specified number of interpolations though out the data set. Linear interpolation is performed between two

consecutive values until the number of interpolations to be performed is reached. The interpolated data sets are: Peak Periodicity (difference in time between two consecutive peak values), Threshold Crossing Periodicity (the difference in time between two consecutive threshold crossings). Heart Rate based on peak times, Heart Rate based on threshold crossings, Peak Velocity Amplitude variability (the beat to beat change in the peak velocity amplitude), and Cardiac Cycle Mean Velocity variability (the beat to beat change in the Cardiac Cycle Mean Velocity amplitude). The first four data series (Peak Periodicity, Threshold Crossing Periodicity, Heart Rate based on peak times, Heart Rate based on threshold crossings) determine the frequency modulation characteristics of the velocity profile. The last two time series (Peak Velocity Amplitude variability, Cardiac Cycle Mean Velocity variability), determine the amplitude modulation characteristics of the velocity profile.

Once the interpolated data sets are formed, the are passed into a sub VI *Detrend.VI*. The sub VI *Detrend.VI* first removes the mean value from each data set, and then determines the best fit to the data (using a 1st order, 2nd order, or 3rd order polynomial, with singular value decomposition (SVD) as the detrending algorithm). The trend is then subtracted from the demeaned data sets.

The data sets then go into the sub VI *Finishing Touch.VI*. The input amplitude array is passed through a 5th order Butterworth low pass filter, with a cutoff frequency of 4 Hz. The user has the option of windowing the data (if the

data is windowed the spectral information will be back corrected to eliminate processing artifact incurred by windowing). The power spectrum of interpolated data sets are determined. If the data is padded the spectra will be scaled accordingly (multiplication by the padded array size divided by the unpadded array size for the amplitude spectrum (or this quantity squared for the power spectral density)). The user has the option of displaying the this spectrum as an amplitude spectrum, or as a power spectral density. The user also has the option of saving the non normalized spectral data and time data to a file.

The frequency and amplitude information for each spectrum is then passed to the sub VI *Normalized Spectra.VI*. The frequency axis of each spectra is normalized by multiplying the frequency array by the threshold crossing mean value. The periodicity spectra are normalized by dividing the periodicity by the threshold crossing mean value. The heart rate spectra are normalized by dividing by the threshold crossing mean value. The amplitude and mean cardiac cycle velocity are normalized by cardiac cycle mean value. If we were calculation normalized power spectral densities, the normalization factors for the amplitude values would be squared. The spectral information can be saved to file.

Appendix E

E.1 Demodulation Test Signals

In order to test the demodulation algorithm, two test signals were crafted. These signals were acquired and processed using the algorithms that were developed for this thesis.

The first test signal was a sine wave having an amplitude of 1 V_{p-p}, and a frequency of 1000 Hz. For details on the demodulation algorithm see sections 4.2, and D.2.2. Since the test signal is a single tone, we expect to see a flat line because the dominant frequency of every packet will be the frequency of the single tone (see Figure E-1).

Figure E-1

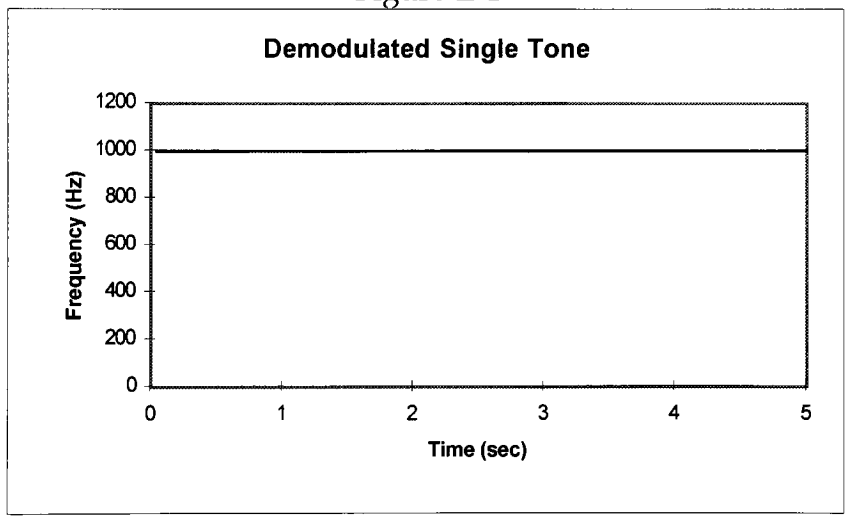

The second test signal was a swept sine wave having an amplitude of 1 V_{p-p}, sweeping linearly in frequency from 100 to 1000 Hz. Since the test signal's frequency increases linearly, we expect to see a ramp for the resulting

demodulated time series. This is due to the fact that the dominant frequency of the data packets will be changing linearly over time (see Figure E-2).

Figure E-2

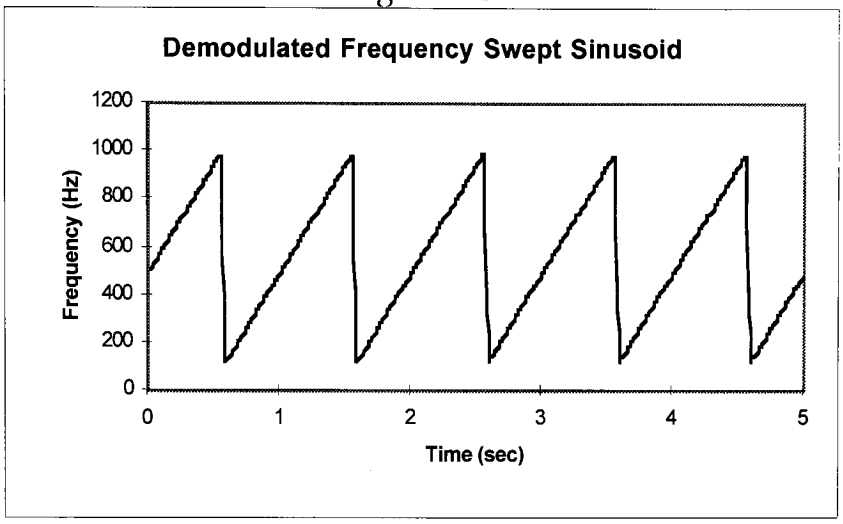

E.2 Processing Tests

In order to assess the effects of changes in the physiologic spectra due to shifts in the time series, various portions of the Peak Velocity Amplitude Variance time series shown in Figure 33 were extracted, and the spectra of the new time series were evaluated. Figure E-3 shows the amplitude spectrum for the unaltered time series. The dominant peaks in the spectrum occur at .0945 Hz, and .4723 Hz, respectively.

Figure E-3

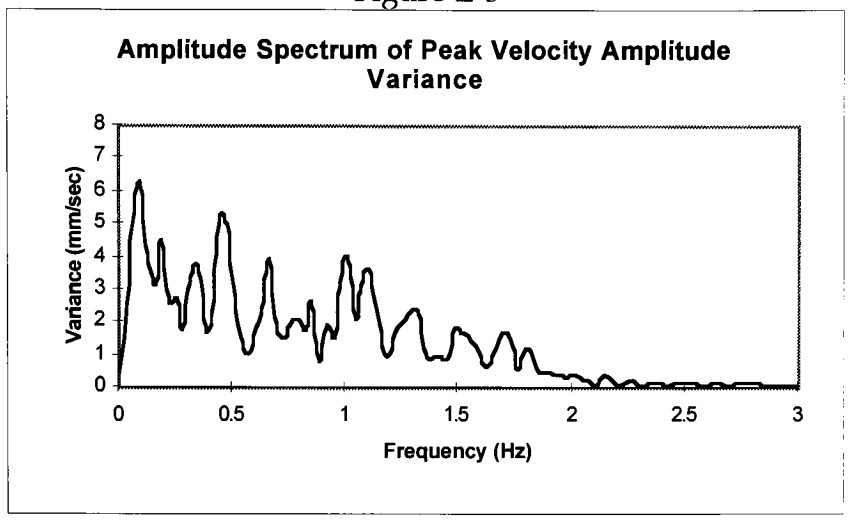

Figure E-4 shows the amplitude spectrum of an altered version of the Peak Velocity Amplitude Variance time series. In this case the first 10% of the time series was removed. The dominant peaks in this spectrum occur at .0709 Hz, and .9928 Hz, respectively.

Figure E-4

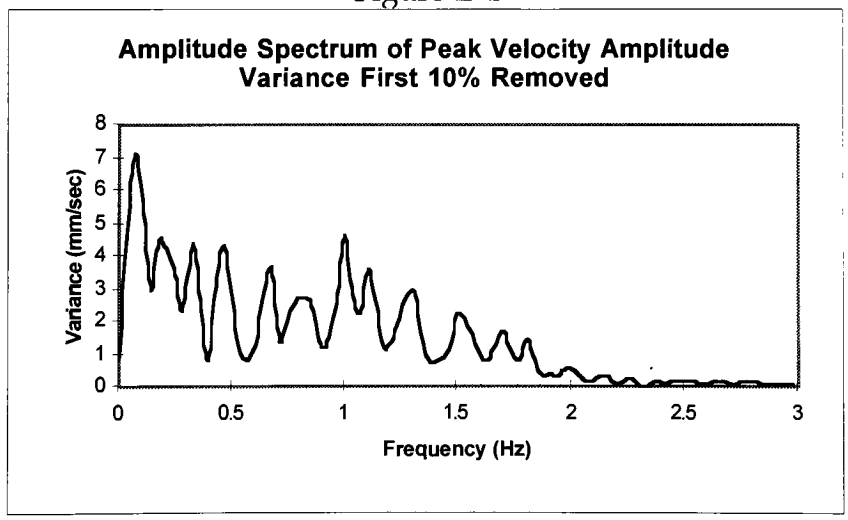

Figure E-5 shows the amplitude spectrum of an altered version of the Peak Velocity Amplitude Variance time series. In this case the last 10% of the time series was removed. The dominant peaks in this spectrum occur at .4672 Hz, and .1078 Hz, respectively.

Figure E-5

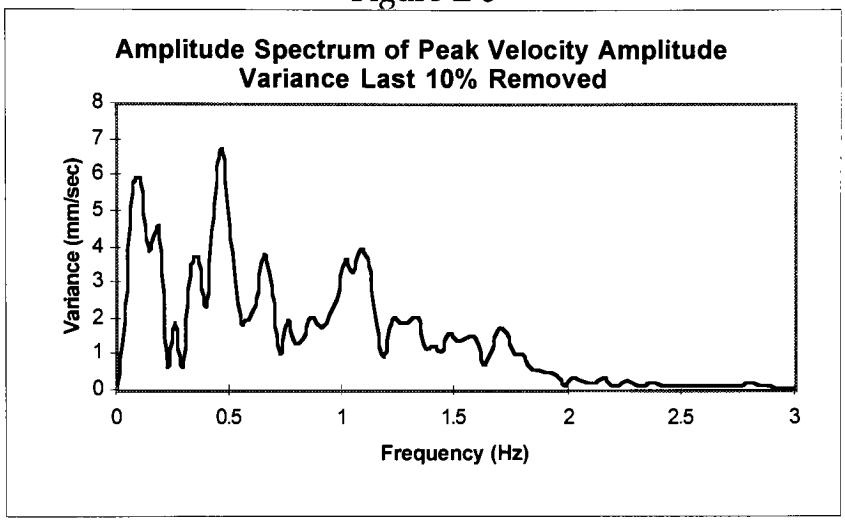

Figure E-6 shows the amplitude spectrum of an altered version of the Peak Velocity Amplitude Variance time series. In this case the first and last 10% of the time series was removed. The dominant peaks in this spectrum occur at .0901 Hz, and .4507 Hz, respectively.

Comparison of Figures E-4 through E-6 shows that the spectral content revealed by Fourier analysis is a modest function of the data segment chosen for analysis. As such, we speculate that the original data record size for Figure 33 (32 sec), may not be adequate to reveal the underlying low frequency variability in that physiologic signal.

Figure E-6

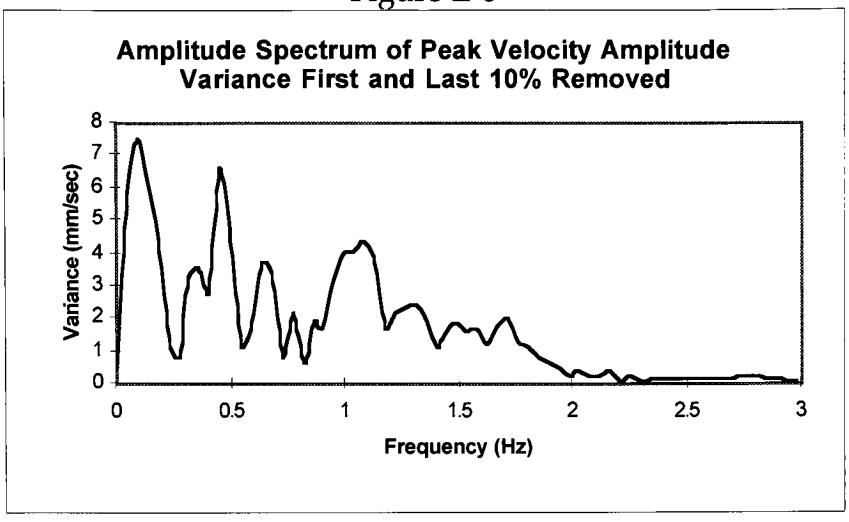
Amplitude Spectrum of Peak Velocity Amplitude
Variance First and Last 10% Removed
Variance (mm/sec)
8
7
6
5
4
3
2
1
0
0
0.5
1
1.5
2
2.5
3
Frequency (Hz)